nature communications

Article

https://doi.org/10.1038/s41467-025-60122-8

New information triggers prospective codes to adapt for flexible navigation

Received: 5 September 2023

Accepted: 13 May 2025

Published online: 24 May 2025

Check for updates

Stephanie M. Prince, Sarah Danielle Cushing, Teema A. Yassine, Navya Katragadda, Tyler C. Roberts & Annabelle C. Singer

Navigating a dynamic world requires rapidly updating choices by integrating past experiences with new information. In hippocampus and prefrontal cortex, neural activity representing future goals is theorized to support navigational planning. However, it remains unknown how prospective goal representations incorporate new, pivotal information. Accordingly, we designed a navigation task that precisely introduces new information using virtual reality, and we recorded neural activity as male mice flexibly adapted their planned destinations. Here we show that new information triggered increased hippocampal prospective representations of both possible goals; while in prefrontal cortex, new information caused prospective representations of choices to rapidly shift to the new choice. When mice did not adapt, prefrontal choice codes failed to switch. Prospective codes were dependent on the amount of behavioral adaptation needed; the new goal arm was represented more strongly when animals needed to change their behavior more. Thus, we show how prospective codes update with new information to flexibly adapt ongoing navigational plans.

The ability to rapidly update our choices in response to new information is essential to navigating a dynamic world. During navigation, animals often hold an internal representation of their world via a cognitive map[1–3]. When navigation is goal-directed, this internal model is employed to represent not only current state information, but also upcoming choices or possible actions to reach a goal. Current theories propose that these prospective representations of future choices are a neural correlate of planning or deliberation, to simulate consequences of potential actions before they occur[4–10]. Such theories imply that these prospective codes facilitate flexible navigation in which animals continuously select from potential choices as events unfold. However, many of the studies testing prospective codes occur in static environments where animals do not need to adapt their behavior within single trials after their initial choices have been made. In dynamic environments where sensory stimuli change frequently, animals must continuously assess new information to inform their decisions and update choices as needed. Thus, it is unclear how prospective codes contribute to flexible navigation that requires continuous assessment of and responses to new information.

Hippocampus, which is essential for spatial navigation, is classically known to encode animals' current position in an environment, but research has also found that non-local representations occur during active navigation. Prior studies have shown that sweeps of coordinated place cell activity tile the space behind and in front of animals during behavioral hallmarks of deliberation[11,12]. During active behavior, individual neuron activity as well as population-level sequences can represent non-local positions stretching far in front of and behind the animals[13–21]. One theory is that these sequences and sweeps reflect upcoming choices or might steer behavior toward a specific goal, but the degree to which choices can be predicted from this activity is inconsistent across studies[22,23]. Another theory is that these non-local position codes are not just representations of animals' upcoming choices but are instances of hippocampus presenting all possible hypothetical paths. This constant path simulation might allow animals to quickly consider and decide between potential options, a cognitive process that would be especially valuable in dynamic environments where new sensory information changes which potential plans are optimal. Overall, it remains unclear why non-local

Coulter Department of Biomedical Engineering, Emory University and Georgia Institute of Technology, Atlanta, GA, USA. e-mail: asinger@gatech.edu

representations have been observed to sometimes predict upcoming behavior and at other times reflect both options equally.

During goal-directed navigation, animals must not only encode spatial trajectories through their environment, but they must also select and maintain choice information as their trajectories unfold. Prefrontal cortex is thought to represent upcoming choice information and is required for flexible decision-making. In the context of spatial navigation, several studies have found evidence that prefrontal cortex acts in coordination with hippocampus to facilitate decision-making and planning for upcoming choices[24–29]. Prefrontal cortex neural activity in rodents has been observed to co-occur with hippocampal activity specifically when hippocampus encodes non-local spatial representations, suggesting prefrontal cortex may play a role in evaluating these non-local codes as potential choices[20,30,31]. Indeed, hippocampal-prefrontal spatial representations in rodents are more coordinated when both regions are representing upcoming choices, and inactivating prefrontal cortex disrupts hippocampal prospective codes and sequences[32–34]. However, the question remains, what are the roles of hippocampus and prefrontal cortex in a dynamic environment that requires flexible decision-making and reconsideration of potential choices? It is unclear how these hippocampal non-local codes and prefrontal cortex choice representations respond to new information to accurately update decisions when plans need to be changed.

To address these open questions, we designed a memory-based decision-making task in virtual reality. In this task, we precisely controlled the timing of new information in the environment on a single-trial basis; animals were required to consider two possible paths and flexibly change course mid-trial when new information indicated a switch in the location of the rewarding outcome. We then recorded many units from hippocampus and prefrontal cortex in male mice during this behavior in order to evaluate how prospective codes respond to new information that demands flexible navigation. We assessed prospective codes for goal locations and upcoming choices using a Bayesian decoding approach, decoding the animal's position and evolving choice from neural activity. In hippocampus we found that new, pivotal information causes non-local representations of both possible goal locations to rapidly increase. In prefrontal cortex we found that new, pivotal information causes choice codes to rapidly switch to represent the new choice. We then identified how prospective codes differed when animals failed to adapt; hippocampal position codes remained relatively intact but prefrontal choice codes did not switch to represent the new choice more strongly than the old choice. Finally, we assessed the neural responses as a function of how strongly animals were committed to their choice before new information was presented. In hippocampus, the introduction of new, pivotal information increased representation of the new goal location when animals were more committed to the prior goal arm and a larger behavioral adaptation was needed to change to the new arm. In prefrontal cortex, we found representation of the initial arm choice decreased more and representation of the new arm choice increased more when more behavioral adaptation was needed upon presentation of the new, pivotal information. These results reveal how prospective codes support flexible planning and accurate decision-making in the face of new information, and how prospective codes rapidly change to represent both possible options or upcoming choices depending on the degree of behavioral commitment.

Results

Animals rapidly update their choices in response to new information in a spatial memory task

To investigate how animals update plans when presented with new, pivotal information, we designed a virtual reality spatial navigation task (Fig. 1a). Mice ($n = 7$ animals) were trained to navigate a y-maze using visual cues displayed on the wall (see Methods for training paradigm). The first original cue, presented on the walls in the central arm of the track, indicated which arm of the track (left or right) was the rewarded location. On most trials (65%), the original cue then disappeared when mice reached a specific location in the track, and the cue was replaced with uninformative gray checkered walls for the remainder of the trial (delay-only trials). The mice had to maintain the memory of the correct goal arm during the delay period (10.56 ± 0.07 seconds, $n = 7172$ trials, Supplementary Fig. 1). On a subset of trials, a second visual cue appeared when mice reached a specific location after a shortened delay period (1.40 ± 0.03 seconds, $n = 1840$ trials). During the second cue, the visual patterns appeared on the opposite wall from the original cue indicating that the reward location switched from the initial arm, and animals must switch from their initial decision maintained in memory to the opposite choice (switch trials, 25%). The second visual cue was then followed by another delay period before the reward location (6.02 ± 0.08 s). On switch trials, the correct goal switches from the initial to new arm, while on delay trials, the correct goal arm is always the initial arm. The remaining 10% of trials were stay trials, which will be discussed in later sections. Delay-only, stay, and update trials were randomly presented. After several phases of behavioral training, animals learned to remember and follow the cues across all trial types and performed above 50% accuracy (delay only mean ± SEM: 65 ± 2%, switch mean ± SEM: 74 ± 2%, $p = 6.197e{-}10$ delay only vs. 50% correct, $p = 3.410e{-}11$ switch vs. 50% correct, Fig. 1b, Supplementary Fig. 1b). Performance was slightly worse overall on delay only trials, likely due to the longer delay duration between the original cue and reward compared to update trials. Indeed, behavioral performance varied as a function of delay duration during brief warm-up periods at the start of each session (Supplementary Fig. 1c). Overall, these results show animals successfully perform both flexible and memory-guided decision-making in this spatial navigation task.

Given our central question about how prospective codes respond to flexible navigation demands, we were specifically interested in the behavior around the update cue on the switch trials, when animals had to update their behavioral trajectories in response to new information. The animals' heading direction (view angle, see Methods) slowly diverged on average as animals approached the ends of the track (Fig. 1c). We found that on switch trials around the update cue onset, the animals' heading direction shifted from one direction to the opposite in response to the cue indicating the reward location had changed (Fig. 1d, see Supplementary Fig. 1d for other behavioral metrics). These behavioral data show that animals rapidly switch decisions in response to new information.

Enhanced non-local codes of both goal locations in hippocampus in response to new, pivotal information

To determine how prospective codes change with new information in a dynamic environment, we recorded single unit and local field potential activity in dorsal hippocampal CA1 and medial prefrontal cortex during behavior ($n = 3892$ units in hippocampus, $n = 2557$ units in medial prefrontal cortex, Fig. 1e, Supplementary Fig. 2a, b, Supplementary Table 1). As expected from prior literature, we found that neurons in both hippocampus and prefrontal cortex had spatial tuning curves that tiled the virtual environment (Supplementary Fig. 2c, Supplementary Fig. 5a). To determine if prospective codes of position represent possible paths or planned paths in response to new information, we estimated population-level representations of position using memoryless Bayesian decoding of hippocampal and prefrontal activity (see Methods). We first confirmed that hippocampal and prefrontal activity could reliably decode the animals' current location in the environment; decoded positions from neural activity represented the animals' true position across locations in the environment (Supplementary Figs. 2d and 5b).

We used this decoding approach to understand how neural representations change when animals receive new information that

https://doi.org/10.1038/s41467-025-60122-8

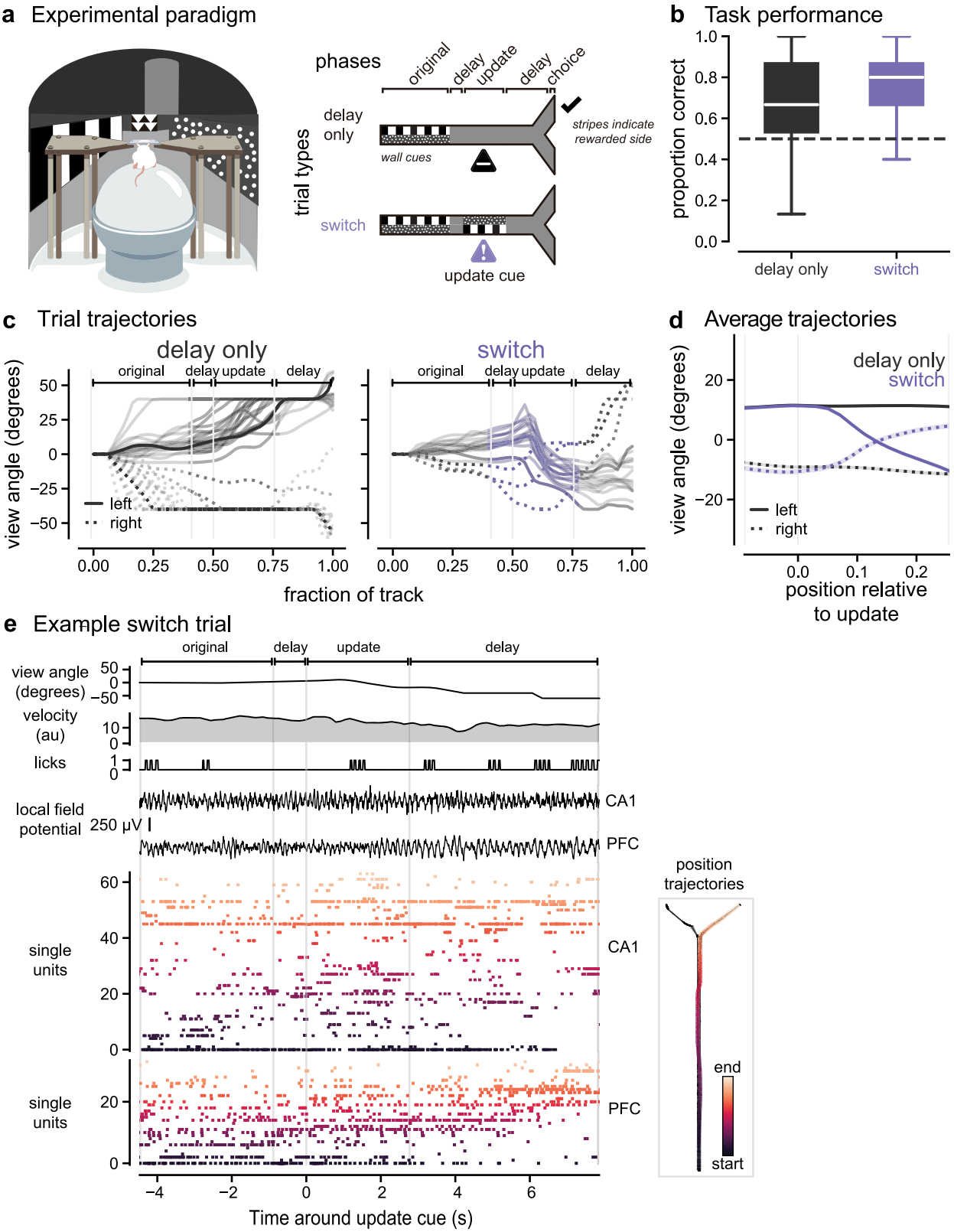

directs them away from a previous goal destination to a new goal location. To do so, we focused specifically on neural activity around the update cue onset. We expected that neural activity in hippocampus would predominantly represent animals' current position, but there would be some remote prospective position coding[19–21,35]. We hypothesized that the amount of non-local representation would remain constant, and both goal locations would be represented equally in hippocampus while animals were in the central arm of the track, even when new information was presented. Before the update cue onset and on delay-only trials, decoded positions predominantly represented the animals' current position (Fig. 2a, b). In contrast, we were surprised to observe that shortly after the update cue was presented on switch trials, the decoding output rapidly jumped from predominantly representing the animals' current location, to representing non-local

Fig. 1 | Mice rapidly and selectively update their choices in response to new information. a Update task paradigm with cues on track walls (left) and trial types (right). Delay only trials (black triangle) featured an original cue followed by a delay with no cue. Switch trials (purple triangle) featured an original cue, a brief delay, and a second cue period during which cues appeared on the opposite wall as the original cues. Check marks indicate rewarded side. **b** Proportion correct delay only (black) and switch (purple) trials ($n = 7$ mice). Box plots indicate median and quartiles of 40-trial bins. (delay only: 0.68 ± 0.00, $n = 6252$ windows of 40 trials; switch: 0.78 ± 0.01, $n = 1002$ windows). Linear mixed effects model (LME), see Supplementary Table 2. **c** Example behavioral trajectories. View angle across track locations for example correct left (solid lines) and right (dashed lines) trials. Gray vertical lines indicate task phases. View angle is set to 0 at trial onset. On update trials, purple indicates periods around the update cue. **d** Average view angle trajectories across all delay (gray) and switch (purple) trials. Dashed lines: initial right trials, solid lines: initial left trials, mean ± SEM. **e** Example behavior (view angle, velocity, licks) and electrophysiological recordings from hippocampal CA1 and medial prefrontal cortex (PFC). Local field potential from the channel with the peak sharp-wave ripple power in CA1. Single units, including putative pyramidal cells and interneurons, darker colors indicate place fields earlier in the track, lighter orange colors indicate place fields at the end of the track. Data shown from 3 s after trial start until animals reach the end of the chosen arm. 2-dimensional position trajectory for the same trial (right). Darker orange colors indicate earlier position and lighter colors indicate later. Other spatial trajectories for the same session are shown in black. ns, not significant, $^{*}p < 0.05$, $^{**}p < 0.01$, $^{***}p < 0.001$, $^{****}p < 0.0001$. Mean ± SEM reported in parantheses. All statistical tests were two-sided. Source data are provided as a Source Data file.

locations within both the new and initial goal arms (Fig. 2a, b). Note that we compared switch and delay only trials that had the same original cue, and we refer to "initial" and "new" arms for the sake of comparing to the switch trials. On delay only trials the initial arm is the one that is ultimately rewarded, while on switch trials the new arm is the one that is rewarded. We quantified this elevated non-local representation and found that the overall probability of goal locations being decoded, the posterior probability integrated over each goal arm, was elevated on switch trials compared to delay only trials (p = 2.630e-8, initial, switch vs. initial, delay only, $p = 4.157e{-}7$, new, switch vs. new, delay only; in order to assess statistical significance while appropriately accounting for repeated measures within animals and within sessions, we used a linear mixed effects model (LME) approach, see Methods and Supplementary Table 2 for additional statistical details, Fig. 2c–e, Supplementary Fig. 4). This elevation of non-local coding in response to new, crucial information was contrary to our expectations, because we predicted the amount of non-local coding would remain relatively stable throughout the trial similar to what we observed during delay only trials. We then wondered if both goals were equally represented, consistent with a role for prospective codes representing possible paths. We found both the new correct goal location and the initial correct goal location increased similar amounts on average. Overall, these results show that when new, crucial information is presented that requires animals to update their goal destinations, hippocampus suppresses local position coding and increases non-local coding of both potential goal locations.

We asked if prospective coding for the new and initial goal arms increased to represent both arms simultaneously or at different times. To distinguish between simultaneous and separate representations of goal locations, we determined whether each 200 ms bin in each trial more strongly represented one goal arm or a mixture of both arms by computing a goal arm bias index (see Methods). Within these short time periods, each bin strongly represented one arm or the other with 43% of bins highly biased for one arm or the other (having a goal bias index close to 1 or −1), rather than representing a mix of both arms simultaneously (Supplementary Fig. 2e). Interestingly, examining this goal bias index per trial instead of per 200 ms bin, we find both goal arms are typically represented within a trial (with the goal bias index falling between −0.5 to 0.5 for 70% of trials, Supplementary Fig. 2e). Indeed, when we compared differences between the amount of initial goal location and new goal location representations on a trial-by-trial basis, the differences were not significantly different from zero and were not significantly different between switch and delay only trials ($p = 0.7806$ switch vs. delay only, Fig. 2e, see Supplementary Table 2 for additional statistical details). Thus, we conclude that the update cue causes increases in prospective codes for both goal arms with representations of each arm alternating within a trial. As a result, both goal arms are represented within a trial, but they are not represented simultaneously.

We then determined if the update cue increased other non-local decoding, rather than specific decoding of the goal arms. Indeed, we noticed some decoding of retrospective positions behind the animals after the update cue was presented (Fig. 2b). Therefore, we compared the decoding of non-local retrospective positions to decoding of the initial and new goal arms. To ensure we excluded decoding of local and nearby positions, we included decoding of the first portion of the track (0–0.15) as a retrospective non-local position. We found that both initial and new goal arms were represented significantly more than retrospective non-local locations after the update cue on switch trials (retrospective vs. initial: $p = 0.04$, retrospective vs. new: p = 0.0011, Supplementary Fig. 3c). Comparing switch and delay only trials, we found that non-local retrospective codes did not differ significantly (retrospective switch vs delay only: p = 0.0513, Supplementary Fig. 3c). In contrast, decoding of the goal arms was significantly higher on switch than delay only trials (Fig. 2e, Supplementary Fig. 3c). Together these results show that the update cue does elicit stronger representations of both goal locations compared to retrospective non-local positions. We trained our encoding model with delay only trials, so that the spatial tuning curves were not influenced by the neural activity that occurred on the update trials and we could accurately assess how neural activity varied on update trials compared to delay only trials. However, we wondered if these results showing increased non-local decoding after the update were due to the fact that our model was trained on delay only trials. To control for this possibility, we also ran the analysis using all trials in the encoding model and found that while there was more accurate representation of the animals' current location during the update cue, the non-local coding results remained similar (Supplementary Fig. 2f). Because the update trials are interleaved with the delay only trials, it is unlikely that these differences are due to spatial remapping, single unit instability, or behavioral disengagement.

When examining non-local decoding throughout the entire trial, we noted that increased decoding of the goal arms was also present during presentation of the original cue. Performing a similar decoding analysis time locked to the presentation of the original cue, we found an increase in goal arm decoding during the original cue that is largely restricted to the very end of the goal arms, different than the pattern of decoding during the update cue (Supplementary Fig. 3a, b). Indeed, during the original cue we found higher decoding of the back half of the goal arm (initial: $p = 4.842e{-}9$, new: $p = 3.919e{-}14$), while during the update cue decoding of the front half of the goal arms was higher (initial: $p = 0.0100$, new: $p = 1.020e{-}7$, Supplementary Fig. 3a, b). Together these results show that while the original cue also elicits increases in goal arm representations, these differ from the goal representations elicited by the update cue.

In prefrontal cortex, we expected that decoding position from neural activity would also reveal representation of primarily the animals' current position with some weaker representation of the remote goal arms. We hypothesized that in the update task, prospective codes for goal locations in prefrontal cortex would switch from the initial goal location to a new one when animals switched their behavioral trajectory. We noticed that the overall decoding output was less

https://doi.org/10.1038/s41467-025-60122-8

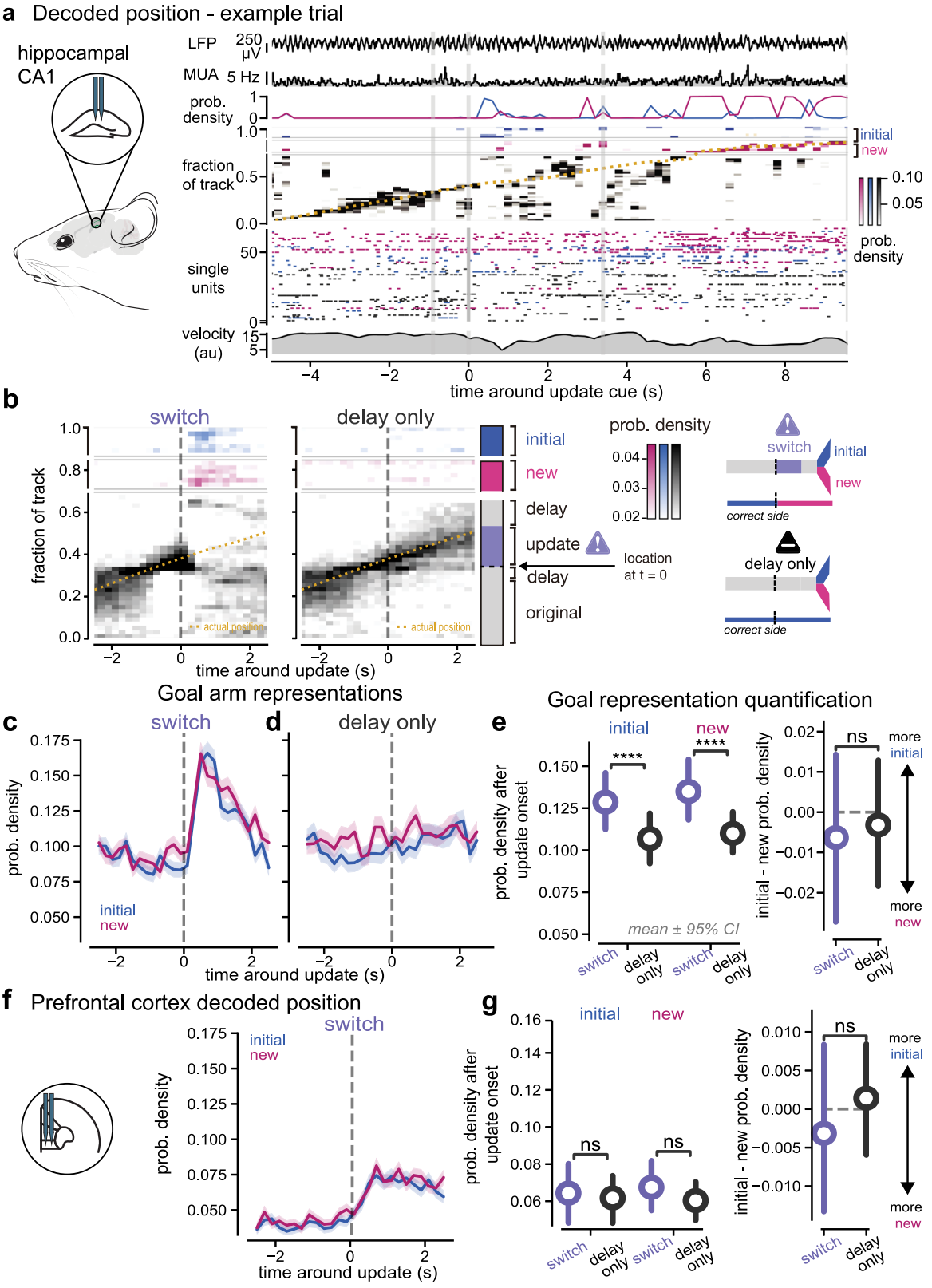

spatially specific in medial prefrontal cortex than in hippocampus. Indeed, we found the spatial spread of decoded positions was significantly wider in PFC than in CA1 (CA1 vs PFC: p = 0.0001, Supplementary Fig. 5f). Furthermore, neural activity in prefrontal cortex represented the animals' current position more than distal locations (Supplementary Fig. 5a–c). Goal locations were more strongly represented in CA1 than in the prefrontal cortex before any changes due to the update cue (CA1 vs PFC initial: $p = 4.641e{-}14$; new: $p < 4.462e{-}61$, Supplementary Fig. 5g). Non-local representations in medial prefrontal cortex were not significantly different across trial types and both goal locations were equally represented until the animals approached the goal arm ($p = 0.3496$, initial, switch vs. initial, delay only, $p = 0.3148$, new, switch vs. new, delay only, $p = 0.9111$, switch vs. delay only, Fig. 2g, Supplementary Fig. 5d). There was a small increase in prefrontal

Fig. 2 | Hippocampal non-local representations for initial and new goals increase in response to new information. a Example hippocampal position decoding on an update trial. Top to bottom: Local field potential (LFP) from CA1, multi-unit activity (MUA), probability density of decoding initial (blue) and new (pink) goal arms, heatmap of decoded locations, single unit activity sorted by place field peak and color coded by largest place field location (black: central arm, blue: initial arm, pink: new arm), summed rotational and translational velocities. Gray vertical lines indicate task timepoints. **b** Decoded positions around update cue for switch and delay only trials, averaged across sessions. Darker color indicates more strongly decoded positions including non-local positions within new (pink) and initial (blue) goal arms (from choice point to end). Yellow line indicates animals' actual position. Schematic illustrates initial and new goal locations and update cue onset (purple). New arm is not visited on delay only trials. **c** Decoding of the new (pink) and initial (blue) goal arms around the update cue on switch trials. Mean ± SEM across trials. **d** As in **c** for delay only trials. **e** Left, decoding of initial and new goal locations after update cue onset on switch (purple) and delay only (black) trials ($n = 1295$ switch, 926 delay only trials; switch: initial: 0.13 ± 0.00, new: 0.14 ± 0.00; delay only: initial: 0.10 ± 0.00, new: 0.11 ± 0.00). Mean ± 95% CI. Right, Within-trial difference between initial and new after the update cue. (switch: −0.01 ± 0.01; delay only: −0.01 ± 0.01). Linear mixed effects model (LME) and ANOVA Tukey post-hoc pairwise test, see Supplementary Table 2. **f** As in **c** for prefrontal cortex position decoding on switch trials. **g** As in **e** for prefrontal cortex ($n = 1109$ switch, 798 delay only trials; switch: initial: 0.07 ± 0.00, new: 0.07 ± 0.00; delay only: initial: 0.06 ± 0.00, new: 0.06 ± 0.00; difference: delay only: −0.00 ± 0.00,; switch: −0.00 ± 0.00). ns, not significant, $^{*}p < 0.05$, $^{**}p < 0.01$, $^{***}p < 0.001$, $^{****}p < 0.0001$. Mean ± SEM reported in parentheses. All statistical tests were two-sided. Source data are provided as a Source Data file.

decoding of goal locations on switch trials versus delay only trials, however these trial types did not differ significantly over several time windows examined (0–0.5 s, 0–1 s, 0–1.5 s after the update cue onset, Supplementary Fig. 5e). In summary, these results show that when new information is presented that requires an update in goal destination, unlike hippocampus, prefrontal cortex spatial representations continue to predominantly represent the animals' current position and do not seem to diverge in representing one goal location over the other until the animals approach the choice point.

Theta phase segregation of non-local and local position codes

Prior studies have shown that local and non-local codes are segregated into different phases of theta oscillations, providing temporal organization and segregation of these different spatial representations. Given the increase of non-local coding we found in hippocampus, we wondered if current and future location codes were segregated by theta phase, as in prior work in static environments without updates[12,13,16,36]. We hypothesized that codes for prospective locations would increase at a specific phase of theta, separate from the phase where local codes dominate, when animals were presented with new information that required them to reconsider potential choices. Using our population-level metrics, we identified the theta phase of each decoded time bin and the corresponding location in the environment (initial goal arm, new goal arm, or central arm). In line with previous work, we found that codes for prospective goal locations (non-local) were represented significantly more on the opposite theta phase as current location representations (local) (p = 0.0275, −π to 0, initial vs. central arm, $p = 0.0106$, −π to 0 new vs. central arm, $p = 9.284e{-9}$, 0 to π, initial vs. central arm, $p = 6.672e{-14}$, 0 to π, new vs. central arm, Fig. 3a–c). Specifically, non-local representations were highest in the first half of the theta cycle, while local representations were highest during the second half of the theta cycle. When comparing before and after the update cue onset, we found that there was a significant increase in the amount of goal location (non-local) decoding, but the local vs. non-local phase preferences were maintained ($p = 6.439e{-14}$, pre- vs. post-update initial arm, p = 5.329e-14 pre- vs. post-update new goal, Fig. 3b–d). Similar to our behavioral-timescale findings, non-local codes at the timescale of individual theta cycles were also significantly larger on switch trials compared delay-only trials ($p = 1.450e{-27}$, initial arm, switch vs. delay only, $p = 1.367e{-13}$ new arm, switch vs. delay only Supplementary Fig. 6). However, in contrast to our longer timescale results, we observed slight differences in initial and new goal codes after the update cue. The new goal location was more strongly theta modulated compared to the old goal location ($p = 0.0008$, new arm $-\pi$ to 0 vs 0 to π, $p = 0.6496$, initial arm $-\pi$ to 0 vs 0 to π, effects were similar when breaking down by quarters, Fig. 3d). Overall, these results show that even with large increases in non-local coding and decreased local coding at longer timescales, non-local goal representations remain segregated from local codes during theta oscillations. While initial and new goals are represented at similar levels in hippocampus at both a behavioral and theta-timescale, stronger theta modulation of new goal codes in particular after the update cue onset suggests more organized spike timing of new goals in response to new, pivotal information.

Rapid switch from old to new choice estimates in prefrontal cortex when new information is presented

While we were surprised that neural activity in prefrontal cortex did not represent the future goal location more than the alternative goal, this may be explained by the overall minimal non-local coding we observed in prefrontal cortex around the update. Because medial prefrontal cortex is known to encode neural correlates of choice in decision-making tasks, we pursued a different approach to explicitly test how the update cue altered choice codes in prefrontal cortex. We hypothesized that in medial prefrontal cortex the choice representation would be stronger for the initial choice preceding the update cue and would then shift from the initial choice to the new choice after the new information was presented. To test this hypothesis, we took advantage of the continuous development of choice that occurs as animals run down the virtual reality environment and is reflected in the animals' changing velocity and heading direction over the course of the track[37]. To obtain a continuous estimate of relative choice commitment throughout the trial, we trained a long short-term memory (LSTM) neural network to predict the mouse's ultimate choice from only the behavioral readouts, specifically velocity, heading direction, and forward position trajectories throughout the trial (Fig. 4a). At each timepoint in the trial, all previous trial time points were used to estimate the animals' final choice. The choice estimate varied throughout the course of a trial, starting at chance-level accuracy at the start of the trial on average, and ending with a highly accurate, or −0.17 ± 0.02 log likelihood on average, prediction of the animals' final choice, where 0 is perfect and −1 is a chance level prediction accuracy (Fig. 4a). We then used this choice measure to obtain a population level estimate of the animals' choice from medial prefrontal cortex using a Bayesian decoder, similar to our previous decoding of position representation (Supplementary Fig. 7a, b).

Using this approach to decode choice from prefrontal activity, we tested our hypothesis that new information causes choice representations in prefrontal cortex to rapidly switch from the old to the new choice. We observed that the choice estimates of the initial and new choice began to diverge preceding the update and then rapidly flipped after the reward location changed ($p = 5.192e{-49}$ initial switch vs. initial, delay only, $p = 2.934e{-7}$ new, switch vs. new, delay only Fig. 4b–f, Supplementary Fig. 7c, Supplementary Fig. 8). Interestingly, on update trials the neural activity rapidly switched from high decoding of the initial choice to high decoding of the new choice, with minimal time spent showing no strong choice estimate (Fig. 4c–e). Furthermore, the difference between initial and new choice decoding was significantly different between switch and delay trial types (p = 8.610e-33 initial − new for switch vs. delay only Fig. 4f). On switch

https://doi.org/10.1038/s41467-025-60122-8

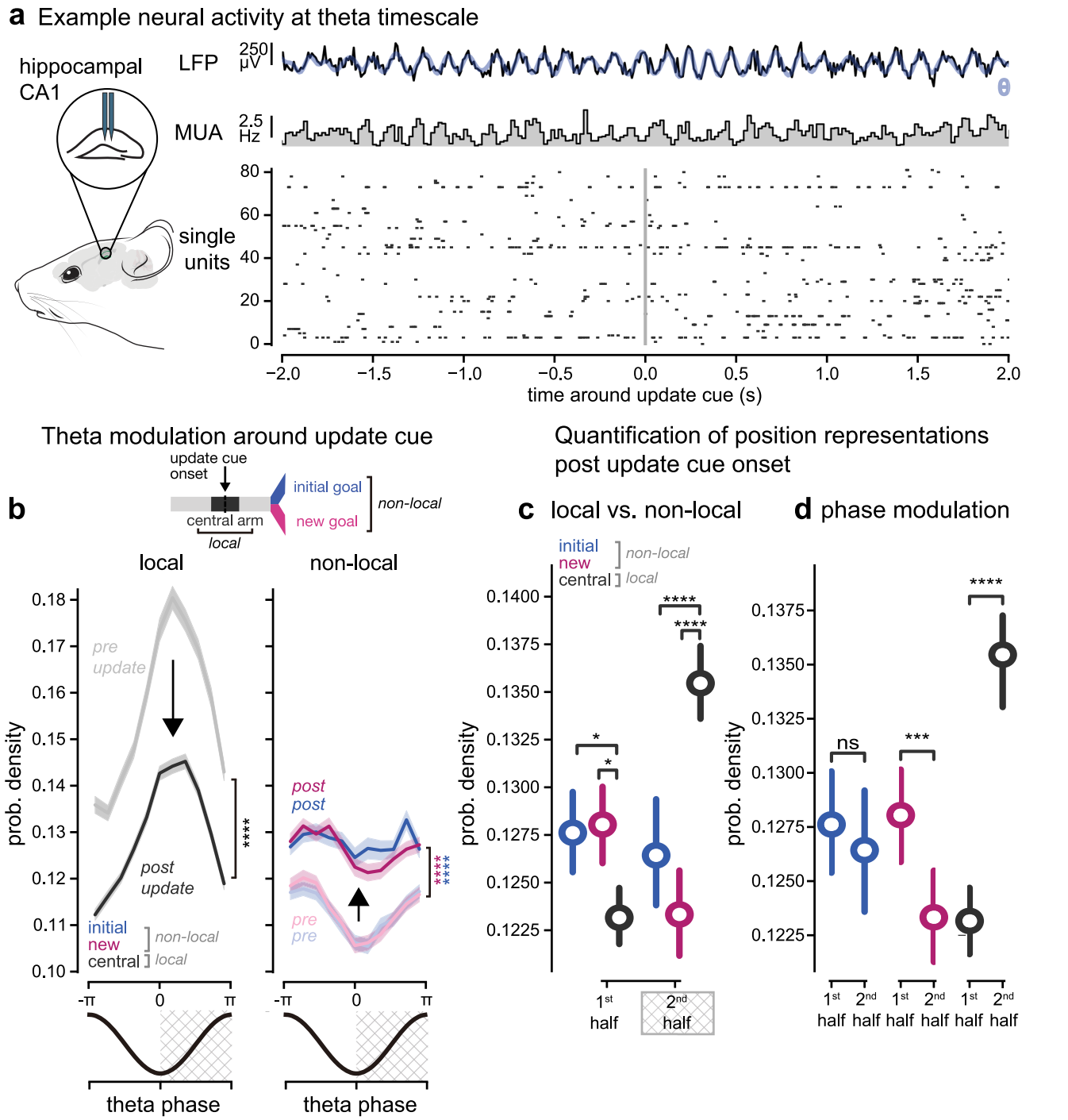

Fig. 3 | Non-local codes occur on distinct theta phases from local position codes and increase with new information. a Top to bottom: Example CA1 theta oscillations (black: low pass filtered, blue: theta band), multi-unit activity, single unit spiking. **b** Average decoded probability densities for central (black), initial (blue), and new (pink) arms as a function of theta phase for local (left) and non-local (right) codes. Pre-update cue (−1.5 to 0 s) in lighter shades; post cue (0–1.5 s) in darker shades ($n = 1295$ trials; initial: pre: 0.11 ± 0.00, post: 0.13 ± 0.00; new: pre: 0.11 ± 0.00, post: 0.13 ± 0.00; central: pre: 0.15 ± 0.00, post: 0.12 ± 0.00). Mean ± SEM across trials. Linear mixed effects model (LME) and ANOVA Tukey post-hoc, see Supplementary Table 2. **c** Probability density of the central (local), new (non-local), and initial (non-local) arm in the first (−π to 0) and second (0 to π) halves of the theta cycle after update cue onset on switch trials ($n = 1295$ trials). Linear mixed effects model (LME) and ANOVA Tukey post-hoc. **d** As in **c** comparing first and second half of theta cycle ($n = 1295$ trials; initial: −π to 0: 0.13 ± 0.00, 0 to π: 0.13 ± 0.00; new: −π to 0: 0.13 ± 0.00, 0 to π: 0.12 ± 0.00; central: −π to 0: 0.12 ± 0.00, 0 to π: 0.14 ± 0.00.). ns not significant, $^{*}p < 0.05$, $^{**}p < 0.01$, $^{***}p < 0.001$, $^{****}p < 0.0001$. Mean ± SEM reported in parentheses. All statistical tests two-sided. Source data are provided as a Source Data file.

trials, after the update cue the new choice decoding was larger than initial choice decoding on average (resulting in a difference that was below zero). Meanwhile on delay only trials, the initial choice decoding was larger than the new choice during the delay where no new information was presented. On average, the change in neural activity choice decoding preceded the movement change (Fig. 4d). Examining when animals began changing head direction (rotational velocity began decelerating away from the initial choice) on a single trial basis, we found initial choice codes decreased and new choice codes increased before the motor response (Supplementary Fig. 7d). Subsequently, the

https://doi.org/10.1038/s41467-025-60122-8

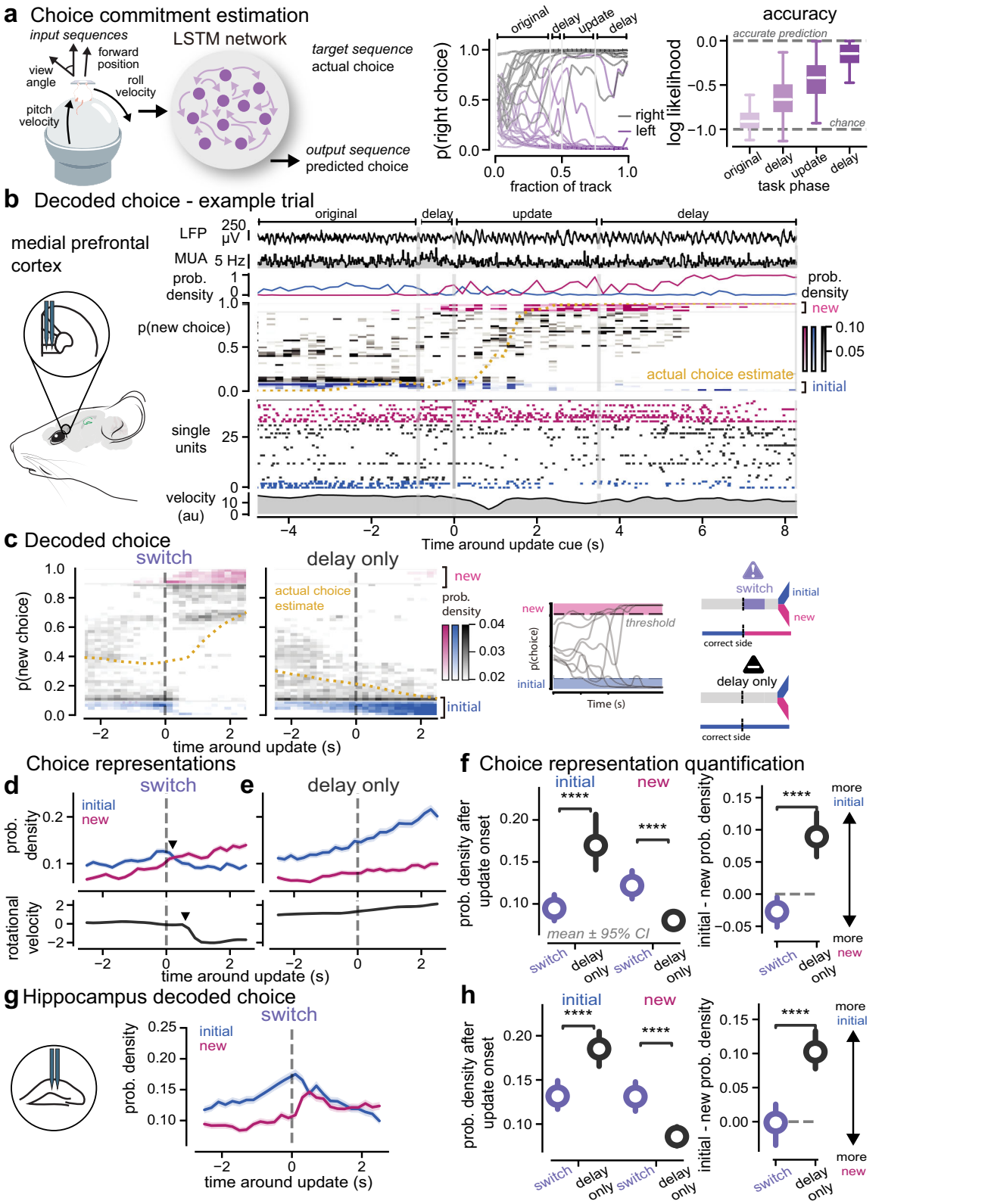

new choice decoding output overtook the initial choice decoding at the same time as the motor response (Supplementary Fig. 7d). Thus, these changes in neural decoding likely precede motor responses and these effects are not likely due to motor response execution. We also found differences in pre-update cue decoding of the initial choices in prefrontal cortex between switch and delay only trials ($p = 0.0031$ switch vs. delay-only 1.5–0.5 s preceding update cue, Supplementary Fig. 7e). These pre-update cue differences likely result from only including correct trials (Supplementary Fig. 7e). Overall, these results show that when animals are presented with new information that required a switch from one choice to another, the new choice is quickly represented more than the initial choice, compared to trials that do not require behavioral flexibility. In contrast to prospective codes for positions in the hippocampus that represented possible paths, these

Fig. 4 | Prefrontal cortex rapidly switches from representing the old to the new choice in response to new information. a Left, Long short-term memory (LSTM) network predicting choice from behavioral trajectories. Center, LSTM output for example left (gray) and right (purple) reported choices. Right, session-averaged log-likelihood indicating LSTM model performance (chance: −1, perfect: 0; $n = 66$ sessions; original: −0.98 ± 0.05; delay: −0.63 ± 0.03; update: −0.43 ± 0.03; delay2: −0.17 ± 0.02). **b** Example update trial. Top to bottom: LFP, multi-unit activity, new (pink) and initial (blue) choice probability densities, decoded choice heatmap, single unit activity with color-coded choice preference (black: no preference, blue: initial, pink: new), summed rotational and translational velocities. Gray vertical lines indicate task timepoints. **c** Decoded choices around update cue for switch and delay only trials, session-averaged. Darker color indicates stronger decoding. Yellow line: actual choice estimate, blue: initial, pink: new choices that reach threshold (see Methods). **d** Decoding of new and initial choice around the update cue on switch trials. Arrow: when new choice exceeds initial. Bottom, rotational velocity. Arrow: first time after cue that change in velocity slope is negative, signifying directional change. Mean ± SEM across trials. **e** As in **d** for delay only trials. **f** Left, initial and new choice decoding post-update on switch (purple) and delay only (black) trials. Mean ± 95% CI ($n = 1109$ switch, 798 delay only trials; switch: initial: 0.10 ± 0.00, new: 0.12 ± 0.00; delay only: initial: 0.17 ± 0.01, new: 0.09 ± 0.00). Right, initial-new difference post update cue (delay only: 0.08 ± 0.01; switch: −0.02 ± 0.01). LME and ANOVA Tukey posthoc, see Supplementary Table 2. **g** As in **d** for hippocampal choice decoding on switch trials. **h** As in f for hippocampus ($n = 1238$ switch, 885 delay only trials; switch: initial: 0.14 ± 0.00 new: 0.13 ± 0.00; delay only: initial: 0.19 ± 0.01, new: 0.09 ± 0.00; difference: delay only: 0.10 ± 0.01, $n = 854$ trials; switch: 0.01 ± 0.01, $n = 1205$ trials). ns not significant, $^{*}p < 0.05$, $^{**}p < 0.01$, $^{***}p < 0.001$, $^{****}p < 0.0001$. Mean ± SEM reported in parentheses. All statistical tests two-sided. Source data provided in Source Data file.

results are consistent with hypothesized roles for prospective codes in guiding behavior.

While the hippocampus is traditionally associated with position more than choice representations, prior work has shown that choice can be decoded from hippocampal activity during decision-making tasks[22,23]. We wondered how new information would affect decoded choice estimate representations in hippocampus (Supplementary Fig. 9a, b). Given our previous results showing equal hippocampal position representations of both goals, we hypothesized that both choices would be represented equally in hippocampus after the update. We found that initial choice representations in hippocampus were higher than the alternative choice preceding the update, and then decreased after the update cue was presented and the new choice representation increased (Fig. 4g, h, Supplementary Fig. 9c, d). However, while the decoded activity followed a similar pattern of switching from the initial to the new choice as in prefrontal cortex, this change evolved over a longer period of time in hippocampus. There was an extended period in which both choices were equally represented in hippocampus, but the choice information had already flipped in medial prefrontal cortex. When quantifying the difference between the amount of initial and new choice representations in hippocampus after the update cue was presented, both choices were represented equally and the difference on a trial-by-trial basis was not significantly different from zero ($p = 0.5625$, initial − new vs. zero, Fig. 4h). Overall, these findings show that new crucial information that requires animals to update their choices results in a switch from old to new choice representations in both hippocampus and prefrontal cortex. However, the representation of both choices converges to similar levels in hippocampus for an extended period of time, while the representation of the new choice more rapidly overcomes the old choice in prefrontal cortex.

Goal codes for updating behaviors are not due simply to new visual information

One of the key concerns we had in the interpretation of our results was whether these differences in goal coding were due simply to the visual change that occurred when the update cue turned on and new information was presented. To control for this possibility, we included an additional set of trials that had the same structure as the switch trials, but the second visual cue was on the same side of the track as initially shown, providing additional evidence that the initial reward location was still correct (stay trials, 10%, Fig. 5a, b). Thus, stay trials included a similar visual cue as on switch trials but no behavioral change was needed. We noted that animals performed very well on stay trials, potentially because the stay cue provides additional evidence that the prior choice is correct and because the delay between the stay cue and choice point is shorter than the delay between the original cue and choice point on delay only trials. Examining hippocampal position coding during the period when prospective codes increase on switch trials, we found that the amount of non-local representations on stay trials was not significantly different from delay-only trials (p = 0.9927, initial, stay vs. delay only; p = 0.6267, new, stay vs. delay only). However, we noticed that there was a transient increase in decoding of the new arm over a short period. Examining that period (0–0.5 s after the update cue), we found significantly more decoding of the new arm on stay trials than on delay only trials (initial, stay vs delay only: $p = 0.9806$; new, stay vs delay only: $p = 0.0375$, Supplementary Fig. 10a, b). These results show that the stay cue elicits a transient increase in representations of the new arm, while the update cue elicits more prolonged increases in representation of both the new and initial goal arms. Non-local codes were in fact significantly lower on stay trials compared to switch trials ($p = 2.358e\text{-}8$ initial, stay vs. switch, $p = 0.0274$ new, stay vs. switch, Fig. 5c, d).

Next, we analyzed prefrontal choice coding on stay trials. We found that new choice coding on stay trials was also at similar levels to delay only trials, and significantly lower than switch trials ($p = 0.7914$, stay vs. delay only, $p = 0.0072$, stay vs. switch, Fig. 5e, f). The decoded initial choice estimate remained relatively constant on stay trials, in contrast to switch trials, though also significantly lower than on delay trials ($p = 0.0032$, stay vs. delay only, p = 1.908e-10 stay vs. switch). Furthermore, the difference between initial and new choice decoding was significantly different between trial types ($p < 4.462e{-}61$ initial−new for switch vs. stay, $p = 0.0033$ initial−new for stay vs. delay only). Overall, these results show that the observed changes in goal codes in hippocampus and prefrontal cortex are not due only to the presence of any additional visual information, but specifically to new, pivotal information that requires animals to update their behavior.

Goal codes predict ability to accurately update decisions in response to new information

After finding that new, pivotal information increased non-local coding for both goal locations in hippocampus and caused a rapid switch from old to new choice codes in the prefrontal cortex, we then asked if these coding adaptations fail when animals do not accurately update decisions. We hypothesized that if increases in non-local goal codes in hippocampus contribute to flexible adaptation of navigational plans, then failure to switch goals in response to new information would co-occur with a failure to increase both non-local goal representations after the update cue is presented. To test this, we compared our population decoding of position in hippocampus and choice in prefrontal cortex on correct versus incorrect switch trials. To account for differences in speed (rotational and translational) as an explanatory variable for the amount of initial and new choice representations, we applied a general linear model (GLM). The residual goal codes from the model were then analyzed to assess changes in goal coding not explained by differences in speed and rotation (Supplementary Fig. 11). We found that indeed on incorrect trials in hippocampus, the new goal choice coding was not as elevated as correct trials (p = 0.0025, new correct vs. incorrect, Fig. 6a, b). However, the difference in new goal choice coding was small and highly variable. There was also no

https://doi.org/10.1038/s41467-025-60122-8

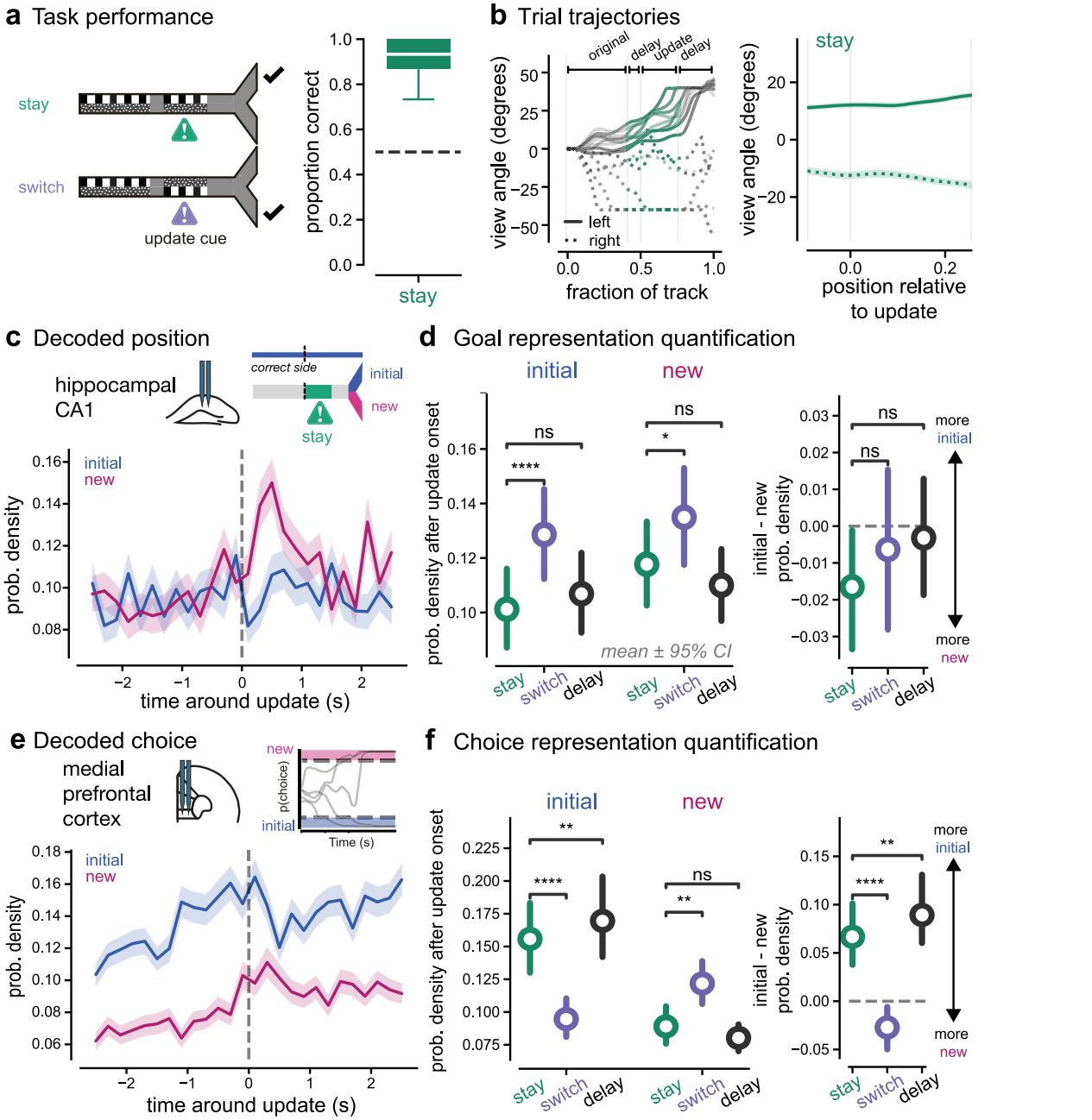

Fig. 5 | Prospective codes for updating behaviors are not due simply to new visual information. a Left, stay trials (green, 10% of trials) consisted of an original cue, a brief delay, and a second cue (green triangle symbol) on the *same* side, unlike switch trials (purple, 25% of trials). Checkmarks indicate correct side. Right, accuracy on stay trials showing median and quartiles ($n = 7$ animals; stay: 0.92 ± 0.01, $n = 117$ 40-trial windows). **b** Left, example behavioral trajectories. View angle for example correct left (solid) and right (dashed) trials. Task phases indicated with gray vertical lines. View angle is set to 0 at trial onset. Green indicates periods around the update cue. Right, Average view angle trajectories across initial right (dashed) and left (solid) stay trials, mean ± SEM. **c** Top, on stay trials, a second cue indicates the initial arm is still correct. Bottom, decoding of new (pink) and initial (blue) goal arms around the update cue on stay trials. Mean ± SEM across trials. **d** Left, decoding initial and new goal locations for first 1.5 s post update on stay (green), switch (purple), and delay only (black) trials. ($n = 551$ stay; stay: initial: 0.10 ± 0.00; new: 0.12 ± 0.01). Mean ± 95% CI. Right, difference on single trials between initial and new probability densities post-update cue (stay: −0.02 ± 0.01). LME and ANOVA Tukey post-hoc, see Supplementary Table 2. Switch and delay only trials in Fig. 2. **e** Top, choice estimate schematic. Bottom, decoding new (pink) and initial (blue) choices around update on stay trials. Mean ± SEM across trials. **f** Left, as in **d** for choice decoding in prefrontal cortex. ($n = 483$ stay; stay: initial: 0.14 ± 0.01; new: 0.10 ± 0.00). Right, within-trial initial and new difference post-update (stay: 0.05 ± 0.01). LME and ANOVA Tukey post-hoc, see Supplementary Table 2. Switch and delay only trials in Fig. 2. ns not significant, $^{*}p < 0.05$, $^{**}p < 0.01$, $^{***}p < 0.001$, $^{****}p < 0.0001$. Mean ± SEM reported in parentheses. All statistical tests were two-sided. Source data provided as a Source Data file.

significant difference in initial goal choice coding on correct versus incorrect trials after the update cue (p = 0.2967 initial correct vs. incorrect, Fig. 6b). Interestingly, preceding the update cue there was a noticeable increase in the initial goal arm representation on incorrect trials that could not be explained by motor differences alone ($p = 0.002$, initial correct vs. incorrect). These results show that when animals failed to switch goals, in hippocampus new goal arm codes did not increase as much in response to the update cue, and initial goal arm codes were elevated before the update cue compared to correct trials.

https://doi.org/10.1038/s41467-025-60122-8

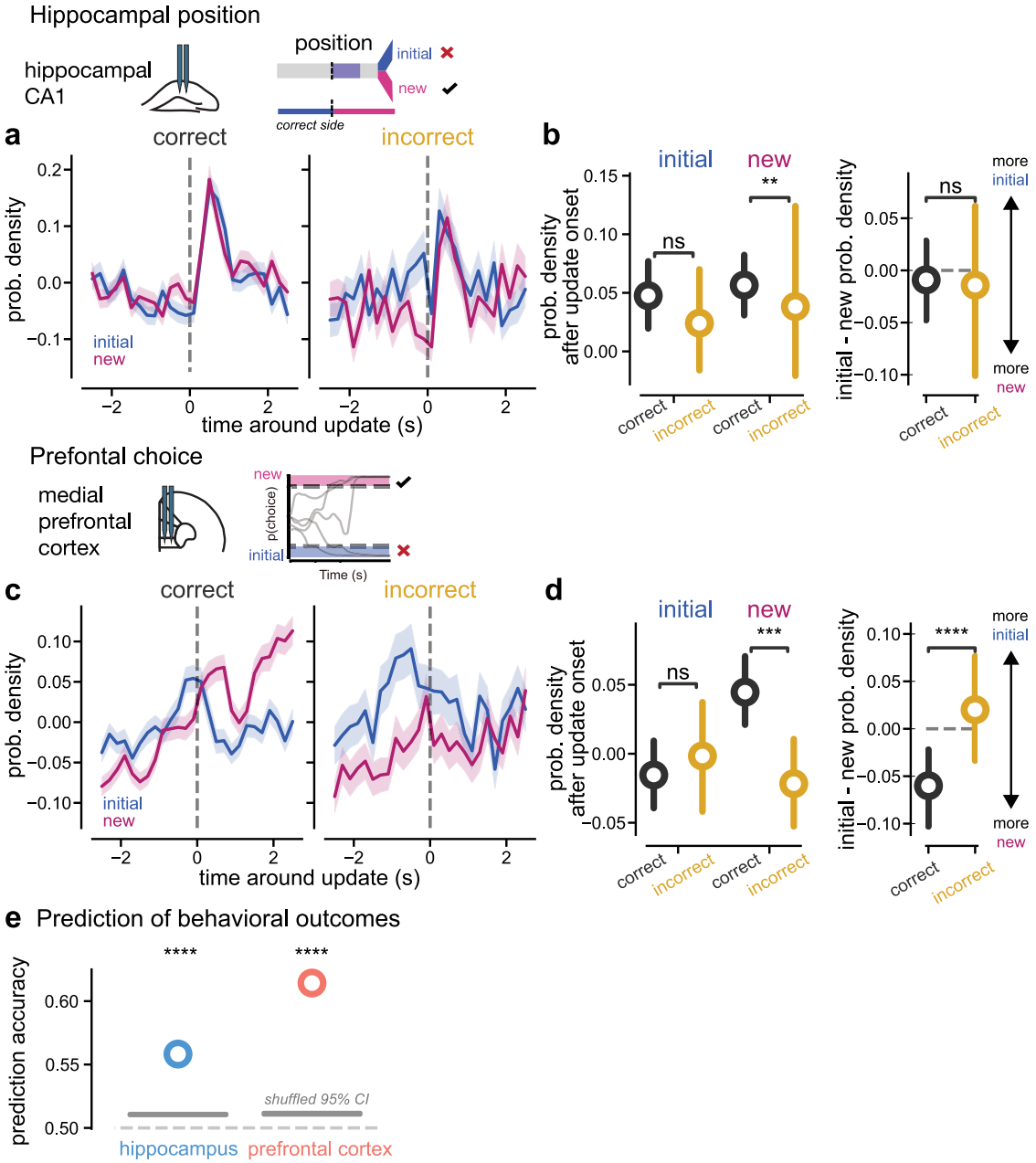

Fig. 6 | Hippocampal and prefrontal prospective codes predict correct responses. a Residual position decoding (probability densities) from hippocampus of new (pink) and initial (blue) goal arms around the update cue on correct and incorrect switch trials. Mean ± SEM across trials. Residuals captured changes in goal coding not explained by differences in speed and rotation in our GLM (see Methods). **b** Left, residual hippocampal position decoding differences after the update cue on correct versus incorrect trials (black: correct, yellow: incorrect). Mean ± 95% CI ($n = 1295$ correct, $n = 407$ incorrect; correct: initial: 0.06 ± 0.01; new: 0.06 ± 0.01; incorrect: initial: 0.03 ± 0.02; new: −0.00 ± 0.02). Right, within-trial initial and new difference after the update cue (correct: −0.01 ± 0.01; incorrect: 0.03 ± 0.02). Linear mixed effects model (LME) and ANOVA Tukey post-hoc, see Supplementary Table 2. **c** Residual choice decoding from prefrontal cortex of new (pink) and initial (blue) choice estimates around the update cue on correct and incorrect switch trials. Mean ± SEM across trials. **d** Left, residual prefrontal choice decoding differences after the update cue on correct versus incorrect trials ($n = 1109$ correct, $n = 359$ incorrect; correct: initial: −0.01 ± 0.01; new: 0.04 ± 0.01; incorrect: initial: 0.01 ± 0.02; new: −0.03 ± 0.01). Right, within-trial initial and new difference after the update cue (correct: −0.05 ± 0.01; incorrect: 0.04 ± 0.02). Linear mixed effects model (LME) and ANOVA Tukey post-hoc, see Supplementary Table 2. **e** Prediction of behavioral choice (correct vs. incorrect) using decoded choice estimates in prefrontal cortex (61.43% accuracy) and decoded position in hippocampus (55.83% accuracy). Dashed lines indicate 50% prediction accuracy, gray lines indicated 95% CI for shuffled predictions. Permutation test, see Supplementary Table 2. ns, not significant, $^{*}p < 0.05$, $^{**}p < 0.01$, $^{***}p < 0.001$, $^{****}p < 0.0001$. All values reported as mean ± SEM. All statistical tests were two-sided. Source data are provided as a Source Data file.

We hypothesized that when animals failed to correctly respond to new information, the new and initial choice representations in prefrontal cortex would fail to flip from the initial choice being more strongly represented to the new choice being more represented. Indeed, we found new choice decoding did not overtake initial choice decoding on incorrect trials (Fig. 6c). This lack of switching choice representations was driven by significantly smaller decoding of the new choice in prefrontal cortex on incorrect trials ($p = 0.002$, new correct vs. incorrect). In contrast, there was no significant difference in initial choice coding on correct and incorrect trials when accounting for motor differences ($p = 0.5874$, initial correct vs. incorrect, Fig. 6d). Similar to hippocampus, the initial choice coding preceding the

update cue was larger on average on incorrect versus correct trials, however in prefrontal cortex these pre-cue differences were not statistically significant when accounting for motor differences ($p = 0.0536$, initial correct vs. incorrect preceding update cue). Comparing new and initial choice representations within single trials, on incorrect trials the old and new choices were decoded at similar amounts even after new information was presented, in contrast to the significantly stronger new choice coding on correct trials (p = 0.0001, initial−new for correct vs. incorrect, $p = 0.3531$ initial−new vs. zero, incorrect trials, p = 0.0113 initial−new vs. zero, correct trials). These results show that when animals failed to switch destinations, initial choice representations decreased in response to new information similarly to correct trials, but there was a failure of the new choice codes to increase in prefrontal cortex after the update cue onset.

We then asked how hippocampal codes for goal arms and prefrontal codes for choice differed on correct and incorrect delay only trials, when animals did not have to update their choice. We compared correct and incorrect delay only trials in the same period as we examined for switch trials. On delay only trials we found no differences in hippocampal decoding of position for either initial or new goal arms (p-values ≥ 0.942), but we did find differences in prefrontal decoding of choice (Supplementary Fig. 12a, b). On correct trials the initial goal arm (the one that will be rewarded on delay only trials) was decoded more strongly than the other goal arm throughout the delay period ($p = 5.934e{-}11$, initial correct vs. incorrect, Supplementary Fig. 12b). On incorrect trials the opposite occurred: the new arm (which will not be rewarded) was decoded more strongly than the initial arm ($p = 0.0002$, new correct vs. Incorrect, Supplementary Fig. 12b).

To test whether these observed codes were related to the animals' behavioral performance, we then used the population measures of goal coding to predict behavioral outcomes on a trial-by-trial basis. We found that in both hippocampus and prefrontal cortex, the population representation of the initial and new goals after the update cue was presented predicted whether the animals would choose the correct or incorrect side (hippocampus: $p < 4.462e{-}61$, prefrontal cortex: $p < 4.462e{-}61$, permutation test, Fig. 6e). It is important to note that the prediction accuracy was lower using hippocampal position decoding (55.83% accuracy) and slightly higher with prefrontal choice decoding (61.43% accuracy). Overall, we found hippocampal and prefrontal goal representations after the update cue onset predicted whether animals flexibly and accurately adapt plans on a trial-by-trial basis as would be expected if these codes were important to the animals' behavioral performance. Together, these results show that when animals fail to adapt to new information, prefrontal representations of the new choice are lacking.

Increased goal representations are correlated with choice commitment

Given that new information triggers a swift increase in hippocampal codes of possible goals and a rapid switch in prefrontal cortex from initial to new choice, we wondered if these changes were directly related to the amount animals must revise their ongoing behavior. We hypothesized that commitment to the initial decision at the time of the update cue onset would influence the degree of modulation of the initial and new goals representations. In other words, if the animals were less committed to their initial choice, the need to consider the alternative goal would be lower compared to trials where they were more committed, and more behavioral adaptation would be needed. To test this, we leveraged a behavioral readout of evolving choice in the virtual reality environment to separate trials with weak or strong commitment to the initial choice. This initial choice commitment was based on view angle at the time the update cue, with the top quartile of view angles (positive values pointing towards the initial goal arm) indicating strong commitment to the initial goal (Fig. 7a Supplementary Fig. 13a). To quantify how position codes were modulated, we measured the change in decoding of the new or initial arm relative to the pre-cue goal representation. In hippocampus, when the animals were more committed to the initial side, the introduction of new, pivotal information resulted in an increased representation of the new, alternative side compared to trials where the animals were less committed or already heading towards the new side. Specifically, the view angle preceding new information was positively correlated with the increase in non-local goal representation of the new arm (new goal codes vs. view angle: $p = 1.330e{-}5$, $r_s = 0.12370$, Fig. 7b, c, Supplementary Figs. 13b and 14e). It is important to note that the correlation between view angle and prospective codes was only observed for the new arm and not the initial arm, suggesting that this relationship is neural content-specific, not simply a general response due to visual cue differences at the time of the update (initial goal codes vs. view angle: $p = 0.1234$, $r_s = 0.0439$, Fig. 7c). In prefrontal cortex, when the animals were more committed to the initial side, the update cue induced a larger decrease in the initial choice representation compared to trials where animals were less committed (initial goal codes vs. view angle: $p = 0.0002$, $r_s = -0.1108$, new goal codes vs. view angle: $p = 0.0414$, $r_s = 0.0615$; Fig. 7d, e). After the update cue, prefrontal decoding of the new arm increased on all trial types, but the increase was the smallest when animals were already more committed to the new arm. Overall, these results demonstrate that greater commitment to the initial choice preceding new information leads to a larger increase of hippocampal non-local coding for the new side in hippocampus. On trials where animals need a larger trajectory adaptation in response to new information, non-local codes for the new goal destination are more prominent. Thus, while prospective codes in hippocampus represent both possible goals, the prominence of a particular goal representation depends on the degree of behavioral change needed.

Discussion

Using a navigation task with precise timing of environmental changes, simultaneous hippocampal-prefrontal cortex recordings, and decoding of position and choice, we determined how prospective codes change in response to new information to guide flexible decision-making. In our paradigm, animals rapidly update their behavior in dynamic environments in response to new information. In hippocampus, our results show that when new, crucial information is presented that requires animals to update their goal destinations, hippocampus increases non-local coding of both potential goal locations. In prefrontal cortex we found new, pivotal information causes choice codes to rapidly switch from representing old to new choices, prior to behavioral responses and prior to choice switching in hippocampus. On incorrect trials, hippocampal non-local goal codes remain relatively intact, but new prefrontal choice coding fails to increase. Furthermore, when animals needed to produce a larger trajectory change, hippocampal representations of the new goal location increased more, while prefrontal representations of the old choice decreased more. Together, these results show that non-local codes are generated in response to new, crucial information that requires flexible decision-making. New information triggers a rapid adaptation of ongoing plans, with hippocampus providing a swift increase in codes of possible goals and prefrontal cortex suppressing initial choices to select a new action plan. When more behavioral adaptation is needed, these prospective codes for new goals are stronger.

Questions about neural correlates of deliberation and planning are often posed within static environments in which behavioral planning is self-driven and internally modulated. However, one of the scenarios in which these codes might be used is rapid adaptation in response to a changing environment. Thus, our central question was how prospective codes in hippocampus and prefrontal cortex contribute to flexible decision-making in dynamic environments. Our results show that in hippocampus, non-local coding for goal locations

https://doi.org/10.1038/s41467-025-60122-8

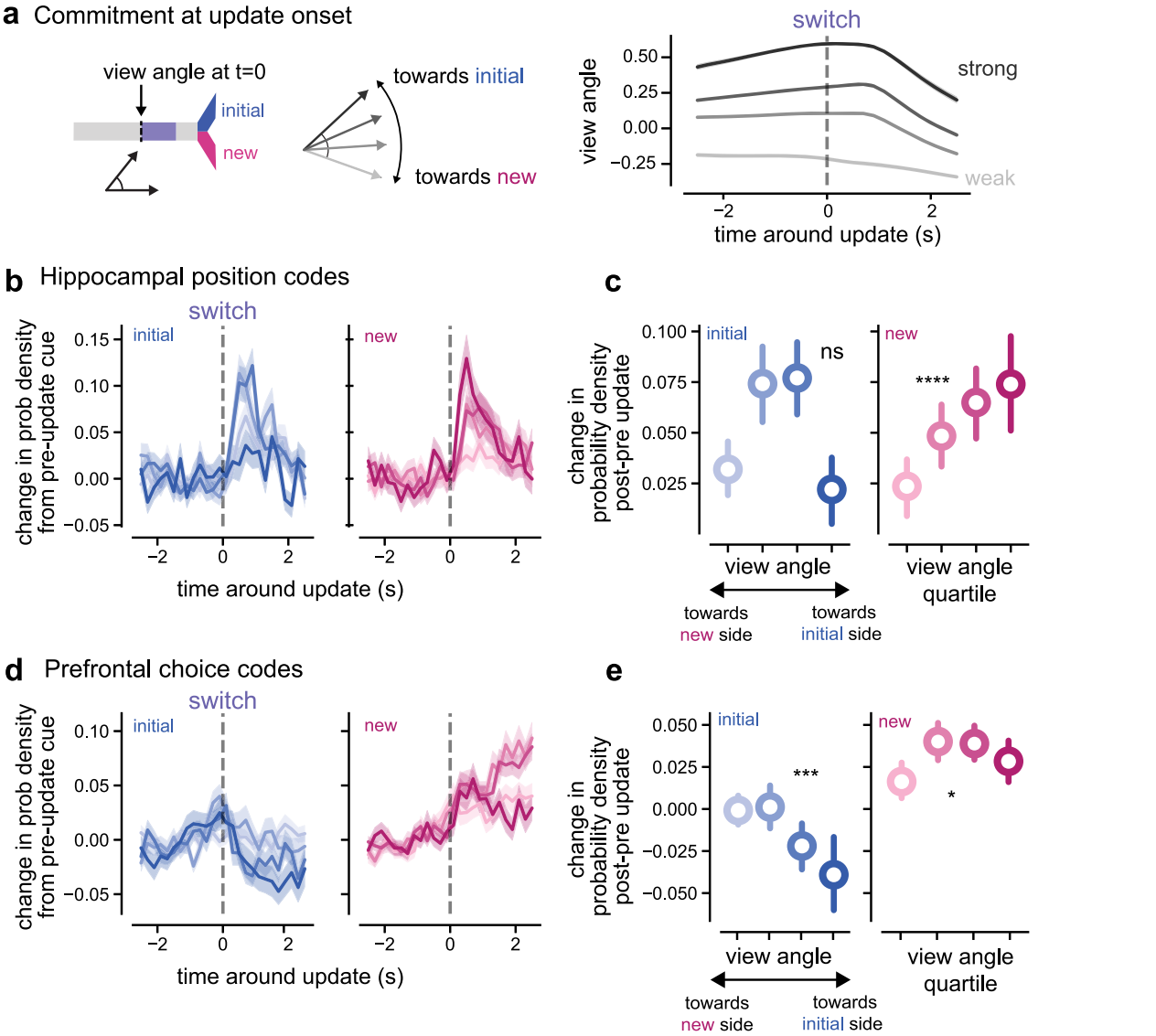

Fig. 7 | Hippocampal codes for new goal locations increase more when animals are more committed to the initial goal. a Left, commitment estimated from view angle at update cue. Right, average view angle trajectories split into quartiles from greatest (darkest) to least (lightest) commitment to the initial side at the update cue. Mean ± SEM across trials, SEM was very small. **b** Change in hippocampal decoding of new (blue) and initial (pink) goal locations relative to before the update cue per commitment quartiles from greatest (darkest) to least (lightest) commitment to the initial side on switch trials. Mean ± SEM across trials. **c** Change in decoding of initial (blue) and new (pink) goal locations per commitment quartiles from greatest (darkest) to least (lightest) commitment to the initial side on switch trials after the update cue. (initial: quartile 1, towards new: 0.03 ± 0.01, n = 410 trials; quartile 2: 0.07 ± 0.01, n = 305 trials; quartile 3: 0.08 ± 0.01, n = 324 trials; quartile 4, towards initial: 0.02 ± 0.01, n = 196 trials; new: quartile 1: 0.02 ± 0.01, n = 410 trials; quartile 2: 0.05 ± 0.01, n = 305 trials; quartile 3: 0.06 ± 0.01, n = 324 trials; quartile 4: 0.07 ± 0.01, n = 196 trials.) Spearman correlation, see Supplementary Table 2. Mean ± 95% CI. **d.** As in **b** for prefrontal choice decoding for initial (blue) and new (pink) choices. **e** As in **c** for change in prefrontal choice decoding (initial: quartile 1, towards new: −0.00 ± 0.00, n = 357 trials; quartile 2: 0.00 ± 0.01, n = 270 trials; quartile 3: −0.02 ± 0.01, n = 286 trials; quartile 4, towards initial: −0.04 ± 0.01, n = 190 trials; new: quartile 1: 0.02 ± 0.01, n = 357 trials; quartile 2: 0.04 ± 0.01, n = 270 trials; quartile 3: 0.04 ± 0.01, n = 286 trials; quartile 4: 0.03 ± 0.01, n = 190 trials.) Spearman correlation. ns not significant, $^{*}p < 0.05$, $^{**}p < 0.01$, $^{***}p < 0.001$, $^{****}p < 0.0001$. All values reported as mean ± SEM. All statistical tests were two-sided. Source data are provided as a Source Data file.

increases when an environment requires a flexible change in action plans. Interestingly, in our task we observe that representations of both goal locations increase similarly in response to new information on correct trials. We did not observe that the planned goal was more strongly decoded than the alternative goal on correct trials until the animals reached the goal arms, tying in with previous work that action plans in rodents are not necessarily predicted by hippocampal prospective codes[21,32,38,39]. Indeed, prior studies and our findings both show CA1 strongly represents position and represents possible paths an animal could take[32]. In addition, we find that when animals must update their planned paths, as on switch trials, hippocampal non-local representations of both goals increase. Thus, our findings show that non-local representations of both goals are not just present but dynamically increase based on task demands. We found some evidence of more subtle differences that might distinguish planned versus alternative choices in the hippocampus; e.g. significant theta modulation of new goal codes compared to non-significant modulation of initial goal codes. In contrast to hippocampus, prefrontal cortex representations of goal locations did not significantly increase when animals had to change their plans. This observation was somewhat surprising because prior work shows that prefrontal cortex activity can represent both planned non-local positions and current position, albeit with lower spatial specificity than CA1[32,40–42]. In agreement with prior studies examining representations of current spatial position, we

find prefrontal cortex exhibits spatial coding but with lower precision than CA1[40]. While the update cue did not induce a significant increase in prefrontal representation of goal arms, such representations may still be occurring and supporting task performance even if they do not dynamically increase with new pivotal information[32,41]. Overall, these results show that hippocampal prospective coding does not preferentially overrepresent the planned trajectory, but a general increase in prospective coding occurs when new, crucial information is presented in an environment.

Importantly, non-local goal coding of the new, upcoming goal increases more when animals need to produce a larger trajectory change in response to the new information. Our findings show that the representation of new possible goals in hippocampus reflects the animals' need to consider new information in relationship to their current decision. These findings may explain variation in the ability to predict upcoming choices from hippocampal activity across studies. We propose that the non-local spiking events might reflect moments of representation of possible outcomes to the animals at a faster timescale scale than other noted behavioral deliberation events such as vicarious trial and error[9,20]. While animals decrease their velocity slightly after the update cue is presented, the animals do not often pause at the update cue or choice point on the virtual reality track and thus do not exhibit traditional vicarious trial and error behavioral features during these moments of non-local coding. These non-local codes might be triggered not only by new information about goals, but also by task-relevant information more generally. Recent work found that neural codes in hippocampus of bats navigating down a tunnel shift to code for distance to other bats that might cause collisions or prompt changes in their trajectory[43]. This detection of relevant non-local stimuli results in a brief decrease in local position representations, similar to our findings. Our results show that non-local coding in hippocampus increases in response to task demands that require planning and flexibility, reflecting the need to consider new information and change behavior.

During flexible decision-making, we find that prefrontal cortex rapidly shifts from one choice to the other, suppressing the initial choice for the new choice to take over. Interestingly, prefrontal cortex choice switching occurs faster than that in hippocampus, suggesting that prefrontal cortex reaches a choice consensus more quickly. Prefrontal choice representational changes also preceded the animals' turning movements on average, though these choice alterations may include some aspects of motor planning. Furthermore, when animals fail to flexibly change their goal destination in response to new information, prefrontal cortex choice representations look very different. In our task, we observe that when the new choice representation fails to overtake the old choice, animals are unable to flexibly respond to changes in the environment. This failure is likely occurring in prefrontal cortex; while non-local codes were disrupted in both brain regions on incorrect trials, hippocampal differences were more variable and had lower predictive power on trial outcomes than prefrontal cortex. However, this study is limited overall in that it does not address how necessary these neural signals from each brain region might be to the animals' behavior. Instead, we manipulated the virtual reality environment to test how sensory information contributes to non-local coding and its role in decision-making. While we primarily focused on the effects of the update cue, the stay cue induced strong performance and neural changes that were distinct from delay only trials. Interestingly, choice decoding of the initial choice decreased after the stay cue and was significantly lower than on delay only trials. Thus, the stay cue likely does not simply increase representations of the initial choice but rather may induce animals to reconsider their ongoing plans. Together, these results suggest that during decision-making in a dynamic environment, prefrontal cortex activity reflects a neural correlate of flexibility in the face of new information.

In summary, this work shows that prospective codes in hippocampus and prefrontal cortex are triggered in response to new, pivotal information in the environment to flexibly integrate new information to adapt navigational plans. We found that new, pivotal information causes rapid increases in prospective coding for non-local positions and switches in coding for upcoming choices and that these codes fail when animals are unable to adapt their previous choices. Furthermore, prospective codes for new goals are more strongly triggered when more navigation adaptation is needed. Thus, by examining neural responses to precisely-timed new information and the degree to which animals adapt to such information, our study provides unprecedented precision in addressing long-standing debates about how prospective codes support deliberation and planning. We propose these non-local codes are neural correlates of planning and consideration of alternative choices that can occur at faster timescales than observable behavioral deliberation and drive neural representations momentarily away from local coding when animals need to adapt their decisions and reconsider potential choices.

Methods

Animals

All animal work was approved by the Institutional Animal Care and Use Committee at the Georgia Institute of Technology. Eight-week-old male WT mice on a C57Bl/6 background were obtained from the Jackson laboratory. Mice were single-housed on a reverse 12-hour light/12-hour dark cycle. Animal housing rooms were equipped with a ventilation system that provides 12 air changes per hour, temperature range of 64–79 °F and 30–70% relative humidity. At the start of the behavioral and electrophysiological experiments, mice were food-restricted to 85% percent of their baseline body weight, and water was provided without restriction. Only male animals were included because this task requires sensitive calibration of the virtual reality behavior system to the size of the animal. Even with this calibration, only some animals are able to learn the task. Fifteen animals total were trained for electrophysiological recordings, one mouse was excluded for lack of movement and inability to complete trials in the visually guided phase, six were excluded for never reaching the final phase of the task (usually due to difficulties in performing over longer delays), and one was excluded after electrophysiological recordings were started due to lack of performance during recording sessions, resulting in seven mice total in the final dataset.

Surgical procedures

Animals were implanted with headplates at approximately 8 weeks of age. Mice were anesthetized with isoflurane before headplate implant surgery. A custom stainless steel headplate was fixed to the skull using dental cement (C&B Metabond, Parkell), and the target craniotomy site for recordings was marked on the skull (in mm, from bregma: −2.0 anterior/ posterior, ±1.8 medial/lateral for hippocampal CA1 and +1.0 anterior/posterior, ±1.25 medial/lateral for medial prefrontal cortex). Craniotomies were later performed before electrophysiology recording sessions in mice that reached the final phase of the task. These craniotomies (200–500 µm diameter) were made using a dental drill to thin the skull and then opening a small hole in the skull with a 27-gauge needle. Craniotomies were sealed with a sterile silicone elastomer (Kwik-Sil WPI) and only opened for recording experiments.

Behavioral task and training

The virtual reality environment was designed using ViRMEn[44] software in MATLAB 2015b and displayed on a cylindrical screen using a projector system reflected by two mirrors. Head-fixed animals ran on a spherical treadmill composed of an 8-inch polystyrene foam ball floating on air. The ball movement was recorded with optical mice and converted to velocity signals in LabView. Pitch velocity was used for forward motion through the environment, and roll velocity was used

for rotational velocity. The view angle was defined as the direction the animals were facing in the virtual reality environment. The start of the trial had a view angle of 0 degrees when the animals were facing straight ahead. View angles began to veer positive (towards the right) or negative (towards the left) as the rotational and translational velocity inputs from the animals' movement on the ball were translated into movement in the virtual reality space. Rewards of sweetened condensed milk (1:2 dilution in water) were delivered via a reward spout and licks were detected using a photo-interrupter.

The behavioral task was a virtual y-maze in which animals had to choose to go to the left or right to receive a reward. The full length of the maze was approximately 3 m for the center arm. Trials were structured as follows: first, the screen displayed the central arm of the environment, and the mouse's position was frozen in place for 3 s to allow the mouse time to adjust its running patterns before it began to move down the track. After this 3 s period, the mouse could begin moving forward, but the view angle and x-position were restricted to 40 degrees and 0 virtual displacement for the first 0.05 fraction of the track. Then, once the mouse passed the initial zone of the track, the mouse could rotate and move freely. The visual cues turned on and off at different locations in the track as the animals passed. On correct trials, a reward was delivered at the end of the track, the VR screen froze for 3 s, and then the task shifted into an intertrial interval period of 6 s. On incorrect trials, the task immediately shifted into a 12-s intertrial interval, which was longer as a form of punishment.

The animals underwent several phases of behavioral shaping and training to reach the final version of the task. In the first phase, animals ran down a linear track that was used to acclimate the mouse to the head-fixed VR setup. The linear track increased in length until the animals completed a certain number of trials for each track length. The second phase of the task was a short y-maze choice task where visual cues indicating the correct and incorrect locations were visible for the full length of the track. After the animals performed two sessions above 75 percent correct, they advanced to the long y-maze choice task with the same visually guided trials as the previous phase but now with the central arm the same length as the final task. Animals were then advanced through phases with a delay at the end of the track. During the delay, the visual cues indicating the correct left or right side were no longer visible and the walls of the track were gray instead. This delay was moved gradually earlier in the track, making it longer in time, through three separate phases. After the animals had reached the learning criteria in the third delay phase, the update cue trials were introduced. In these trials, a second visual cue appeared after the first original visual cue, indicating either the same side as the initial cue or the opposite side. Once the animals showed signs of understanding these second cues, the delay location was moved earlier once more, so that the final update task trial structure had three different trial types. These trial types consisted of delay only trials (65% of trials), in which the initial cue was shown and there was a long delay until the end of the track, switch trials, in which there was an original cue, brief delay, and second cue on the opposite side of the track as the original cue (25% of trials) and finally stay trials, in which there was an original cue, brief delay, and second cue on the same side of the track as the original cue (10% of trials). Recordings occurred once animals showed proficiency with these three trial types: delay only, switch, and stay trials. On recording days animals performed several warm-up trials including short and long delays, but these shorter delay length trials were not included in electrophysiological analyses. The duration of the second delay on stay and update trials was similar to the delay on delay1 trials, starting at 0.57 or 0.56 fraction of the track, respectively (See Supplementary Fig. 1A for task event length information). To control for side biases, the animals' preference for the left or right side of the track, we applied a bias correction algorithm for selecting the next trial type for delay only trials. In short, the probability that the next trial would be on the left or right side was dependent on the history of left and right trial errors. If the animals preferred turning to the right arm at the choice point and had missed mainly left trials, then there would be a higher likelihood of the next trial being on the left, or non-preferred side[45,46]. This algorithm was applied throughout training and during electrophysiological recordings. Animals were trained approximately 5–7 days per week, 1 h per day on average. Overall, this training process took 55.43 ± 7.38 days on average (mean ± SEM, $n = 7$ animals).

Within subject study design, blinding, and replication

We used a within subject design, in which individual animals were exposed to all trial types (delay only, switch, and stay). Due to the nature of experiment monitoring during electrophysiology recording, the experimenter could not be blind to condition. Experimenters were blinded to condition for data processing since all trial types were analyzed together within a session and underwent the same processing pipeline. Sample sizes were not predetermined but are similar to sample sizes used in the field. We recorded from a large number of single units (at least 600 from each animal) from multiple animals and analyzed their activity and determined significance. We repeated the experiments and analyses across multiple animals, serving as biological replicates. Replication was successful. Individual results from individual animals are shown in the supplement.

Electrophysiological recordings

Recordings occurred during behavioral task performance when animals navigated through the virtual reality environment. Data were acquired using a SpikeGadgets acquisition system (Trodes 2.2.2) with a sampling rate of 30 kHz and a ground pellet as reference. Animals were head-fixed on the treadmill for a maximum of one five-hour-long recording session per day (number of sessions ranged from 6–12 per animal, see Supplementary Table 1 for details). A 64-channel, dual-shank NeuroNexus probe was placed in a slightly different location within the craniotomy at the beginning of each recording session and advanced to the target location with the angles of the manipulators adjusted according to the final craniotomy location and target location. In hippocampus, the target location was −1.8 to 2.0 anterior/posterior, 1.5–1.8 medial/lateral, and 1.4 dorsal/ventral. In medial prefrontal cortex, the target location was 1.7–1.8 anterior/posterior, 0.4 medial/lateral, and 2.0 dorsal/ventral. For hippocampal recordings, the probe was advanced to the CA1 pyramidal layer of hippocampus identified via electrophysiological characteristics: large theta waves, sharp-wave ripples, and 150 + μV spikes on multiple channels. Recording sites usually spanned the layer. For medial prefrontal cortex recordings, the probe was advanced to the target location using the distance traveled as the primary metric, until a suitable location was found with the maximum number of spikes.

During the final recording session from each hemisphere, a probe was coated with DiI and inserted to the target depth. Brains were then drop-fixed in 4% paraformaldehyde. Brains were sectioned to either 100 μm thick with a Leica VT1000S vibratome or they were sectioned to 60 μm thick with a Leica cryostat after freezing at −80°. Sections were then stained with 0.2% 1mMol DAPI and mounted on microscopy slides with Vectashield mounting medium. Images were acquired at 10X using a LSM 700 laser scanning confocal microscope (Zeiss). Images were analyzed using Zen Blue (version 3.3) microscopy software. All images with visible DiI were registered to the Allen brain atlas using SHARP-Track[47]. Probe regions of interest were added based on DiI location, isolating individual shanks of the electrode when possible, and the software determined a best-fit line as an approximation of the probe path. The deepest identified point of visible DiI was used to calculate an estimated recording location in the Common Coordinate Framework.

Graphical illustrations of a mouse in VR were created by Bailey Mariner for the Singer lab. Drawings showing a mouse head in profile

(E. Tyler and L. Kravitz, mouse drinking, Zenodo, https://doi.org/10.5281/zenodo.3925985) with a brain (F. Claudi, mouse brain sagittal, Zenodo, https://doi.org/10.5281/zenodo.3925911) were adapted from scidraw.io.

Local field potential and single unit preprocessing

The local field potential was obtained by downsampling raw traces to 2 kHz and bandpass filtering between 1–300 Hz. Outliers were eliminated by interpolating over outliers when the pre-filtered LFP signal was 15 standard deviations above the mean. All LFP analyses used the signal from a single channel that was putatively located in the stratum pyramidale. To identify this channel, the LFP was bandpass filtered for the sharp-wave ripple band (150–250 Hz, see details below) and the average of the sharp-wave ripple band envelope over time was calculated from each channel. The channel with the highest average sharp-wave ripple band power was used for all further LFP analyses, and this channel was predominately located in the middle of the depth-wise span of the NeuroNexus probe.

Spike detection and sorting were performed using Kilosort2 spike sorting algorithm[48] and then were manually curated using Phy software. Cell types were classified into putative pyramidal cells and narrow interneurons and wide interneurons using the default spike width and the autocorrelogram criteria from CellExplorer 1.2 software[49]: narrow interneuron if the trough to peak value was ≤0.425 ms, wide interneuron if the trough to peak value was >0.425 ms and the autocorrelogram tau rise value greater than 6 ms, and the remaining cells were classified as pyramidal cells. The classified distributions of neurons were compared to the ground-truth mouse data provided in the software as a visual confirmation of the accuracy of the classification. Positive spikes were identified with a polarity >0.5 and were flipped for spike width calculations. All cells were visually inspected and a small number (less than 10 total) were excluded if the spike width could not be accurately quantified with the waveform.

Behavioral analysis

To quantify behavioral performance, we binned behavioral data into 40 trial windows for each trial type to calculate a rolling window of proportion correct throughout the behavioral sessions. We also obtained the spatial trajectories of the animals by calculating an average value for each position bin in the environment across individual trials, and then averaging the left and right trials separately to obtain a final average trajectory for each behavioral readout.

For position representation analyses, the 2D position of the VR environment was converted into a 1D linearized position. Linearized position was calculated by generating a graph of the VR environment with 3 segments and 4 nodes: 1 node was at the start of the track, 1 node was at the choice point at the end of the central arm and between the two choice arms, and then the 2 final nodes were at the end of each choice arm. We used the track-linearization package to project each position in the environment using an HMM (hidden Markov map). Artificial gaps between the segments of the track were added for visualization purposes. Data from both left and right trial types were combined.

Locomotion periods were defined as times when the animals' movement was above a velocity threshold. To calculate this threshold, we plotted the distribution of optical mouse recorded velocities and observed a bimodal distribution. We selected a threshold that separated these two distributions and used that for subsequent decoding analyses. Multiple thresholds were tested and the results remained similar.

Choice modeling

To calculate an estimate of choice as animals ran through the environment, we built an LSTM neural network using TensorFlow based on previous choice estimate values obtained in virtual reality two-choice maze tasks[37]. The LSTM network contained a 10-unit LSTM layer, followed by a 1-unit dense layer with sigmoid activation to predict the reported choice at every time point in the trial using the velocities, view angle, and position from that trial up until that time point. The network was compiled with an Adam optimizer and a binary cross-entropy loss function. The input data was a matrix of the rotational and translational velocity signals, the forward position in the maze, and the view angle of the mouse at each time point. A separate model was trained for each behavioral session using a combination of model-averaging and k-fold cross-validation to train and test the model. We divided the data using stratified k-fold cross-validation with 6 folds, in which a separate model was trained for each group of 5 folds and used to predict/test on the 5th fold. The final prediction for each trial was the average of three repeats of this 6-fold cross validation. The training data was normalized and padded to the length of the longest trial, but all trials with a length greater than twice the average were excluded. The hyperparameters of the neural network were selected using a grid search on a subset of the recording sessions and were as follows: batch size = 32, epochs = 20, learning rate = 0.1. Finally, we took the prediction of the model and calculated the log likelihood with log base 2 to assess the overall performance. The prediction data was then used as a feature input to the Bayesian decoding model to assess how the neural activity represented evolving choice as the animals run through the environment. To quantify the performance of the LSTM model and demonstrate how accurately the LSTM model classified the final choice as the animal moved throughout the environment, we used the negative log likelihood. The log likelihood metric measures the performance of a classification model whose output is a probability between 0 and 1, here indicating the probability of the final reported choice being the correct choice. Similar to the negatively signed binary cross-entropy loss that was used for model training, we used the negative log likelihood with a log base of 2 so that −1 would be a chance-level prediction and 0 would be a perfect prediction.

Decoding analyses

To identify a neural representation of different features of the task at a population level, we performed a Bayesian decoding analysis to estimate the probability of different positions or choices given the observed spiking activity at that period. For all decoding analyses, we analyzed hippocampal CA1 and medial prefrontal cortex separately. We first excluded any sessions in which there were less than 20 single units for the brain region of interest and there were less than 50 trials for the behavioral session. These thresholds were chosen by visually inspecting and quantifying the overall decoding accuracy of each session and determining a minimum criteria in which high-fidelity decoding could be obtained. These criteria were applied separately to each brain region (e.g., data from one brain region might be included for the session if it met the criteria, but the other brain region would be excluded if it did not). Brain region decoding outputs were also calculated separately. To build our encoding model, we used only periods within a behavioral trial (excluding the intertrial interval) and only locomotion periods when the animal was moving. We used both correct and incorrect trials but only trials in which there was no update cue. While position decoding used the linearized position of the animal as the encoded and decoded feature, for the choice decoding analyses we used the output of the LSTM network. The output of the LSTM network was a value between 0 and 1 for each timepoint indicating the probability of the final choice being a left or right trial. Feature tuning curves were computed by calculating the number of spikes per feature bin (n = 50 bins for both position and choice features) and normalizing for occupancy time. For decoding, we used 25 ms when analyzing decoding by individual theta phase and 200 ms windows otherwise. To perform the decoding calculations, we used the Pynapple[50] analysis package using a uniform prior. In a subset of our analyses, we used all trial types (delay only, switch, and stay trials) to build our encoding

model as a control. To validate our decoding output, we built the encoding model using 80% of the data and held out a test set of 20% of the data to confirm decoding accuracy across the virtual reality environment.

To calculate representational changes around the update cue, we integrated the posterior probability densities for the initial choice arm and new choice arm based on the boundaries defined by our track graph used for track linearization. We calculated decoding error as the difference between the predicted and actual position. For some analyses, we converted the decoding output into terms of probability density/chance[43,51], where chance was defined as a uniform representation across all spatial bins. This probability density/chance value was obtained by multiplying the probability density function by a uniform constant of 1/the number of spatial bins. With this output, a value of 1 indicates that the decoding output of that bin is the amount expected if all locations were uniformly represented and no location was represented more than others. A value equal to the number of spatial bins would indicate the maximum likelihood of the bin being represented. To calculate representational changes for choice around the update cue, we integrated the posterior probability densities for the initial and new choice based on a threshold. This threshold was applied to identify the highest 10% of all choice estimate values and thus indicate a strong choice representation of either the new or initial choice. We assessed other thresholds and found similar results. We calculated decoding error as the difference between the choice probability predicted from the neural activity and the actual output of the LSTM network.

To quantify the changes in prospective goal coding around the update cue, we calculated the average integrated decoding output value in the 0 to 1.5 s window after the update cue was presented to compare relative amounts of prospective coding between trial types. We also quantified the difference in initial and new goal representation on a trial-by-trial basis to compare relative amounts of initial and new goal representations between trial types. For analyses in which we quantified differences in goal coding preceding the update cue onset, we used the −1.5 to 0 s window as our baseline.

To distinguish between simultaneous and separate representations of goals, we computed the difference in the decoding probability of the new arm and initial arm and divided that by the sum of the decoding probability of the new arm and initial arm. This produces a value from −1 to 1 where −1 indicates only the initial arm was represented, 1 indicates only the new arm was represented, and 0 indicates both arms were represented equally. We refer to this as the goal bias index. A bin was deemed very highly biased to one arm or the other if the goal bias index was greater than 0.93 or less than −0.93 (the highest and lowest bins, respectively, based on binning of the data into 30 bins).

To compare decoding of current position between prefrontal cortex and CA1, sessions with at least 20 cells in each region and 50 trials were included. When one region had a greater number of cells than the other, that region was randomly subsampled to include the same number of cells. Delay only trials were used to exclude the potential effects of the update cue. For decoding spread, the peak value of the posterior probability density function was taken, and one standard deviation was subtracted to define the spread threshold. The spread of the decoded position distribution was defined by how far in front and behind of the peak value the decoding results dropped below this threshold. Prefrontal cortex and CA1 were compared using LMM with session, animal, region, and trial as random effects.

To assess how choice commitment affected neural representations around the update cue, we obtained the view angle at the time of the update cue onset for each trial. We then split this view angle data into quartiles and with these separately grouped trial types, used the same time windows and quantification analysis described above to calculate the average responses. For each commitment quartile, the average decoding probability prior to the update cue was subtracted to quantify how the representation changed with update cue presentation. The decoding probability is also shown in the supplement without subtracting the pre-cue levels.

Heatmaps of decoded position (as in Fig. 2) indicate which positions are most strongly decoded by the spiking activity of all neurons in that region. In the heatmap, each column represents the posterior probabilities of all positions at that point in time. For each column, the position with the highest posterior probability is represented by the darkest shade. Pink and blue indicate decoding of positions within the new and initial goal arms (including the entire goal arms after the choice point), which occurs during the update cue even though the animals are in the center arm away from the goal locations. Animals' actual position is illustrated as a yellow dashed line shown over the same time window. Data from both left and right trial types were combined. Two-dimensional position in the virtual track was converted to a 1D position to disambiguate the new and initial arms of the environment. Schematic to the right of the heatmaps shows locations of the task as shown on y-axis of left panels. Heatmap of decoded choice (as in Fig. 4) show decoding of ongoing choice by the spiking activity of all neurons in that region. In the heatmap, each column represents the probability density function of choices decoded from neural activity at that time point. Pink and blue indicate strong decoding of the new or initial choice, respectively. Schematic of choice estimate thresholds indicates the highest 10% of all choice estimate values and thus indicates strong choice decoding of either the initial and new choices. Animals' actual averaged choice estimate is illustrated as a yellow dashed line shown over the same time window. Data from both left and right trial types were combined. On switch trials the correct goal switches from the initial to new arm, while on delay trials the correct goal arm is always the initial arm.

Theta cycles and phase

For each session, we identified a channel as the putative pyramidal channel in CA1 using sharp-wave ripple power as described above. This channel was used as our LFP recording site. To isolate hippocampal theta oscillations, the LFP was bandpass filtered for theta (4–12 Hz) using an FIR (finite impulse response) equiripple filter. Peaks and troughs of the filtered LFP were detected and used to define the phase of the LFP. In order to use a common theta reference across recording sessions, we calculated a phase histogram of all putative pyramidal cell spiking activity in CA1 for a recording session using 30-degree bins. We then adjusted the theta phase measurement to be 0 degrees at the location of maximal CA1 firing.

To calculate theta phase modulation of goal decoding, we calculated theta phase histograms by identifying the theta phase at the center time of each decoding window and then calculating the integrated posterior probability densities for each theta phase bin for each trial. The analysis time window was based on the previously observed elevation in non-local hippocampal codes from Fig. 2. To compare values across theta, we divided the theta oscillation into quarters and calculated the average decoding output value for each quarter of the theta oscillation.

Generalized linear model (GLM) analysis

To account for the effects of speed and direction on the differences in neural codes between correct and incorrect trials, we applied a GLM with rotational and translational velocities as the explanatory variables or predictors and the goal decoding output as the response variable. A separate model was trained for the different goal representations, initial and new. To fit the model, we used the velocity and decoding output values in 200 ms bins in the 2.5 s before and after the update cue onset across all trial types and animals. We then plotted the Pearson residuals as a measure of the decoding output not

explained by speed and direction differences between trial types. Cox and Snell's pseudo r-squared values were reported as an estimate of model fit.

Prediction of behavioral choice

For prediction of animals' final choice using neural activity, we performed a trial-by-trial classification analysis using support vector machines (SVMs). For each region and update trial type, we trained independent SVMs. For each trial, we used the quantification of goal representation difference between the initial and new goal as described above as a feature (n = 1, initial − new) to predict the animals' final choice (k = 2, correct or incorrect). Before training the classifier, we balanced the correct and incorrect trial classes using random resampling with replacement until both target classes had the same number of trials. We used a radial basis function (Gaussian) kernel for all SVMs, and we selected the hyperparameters (C and γ) using a random search method with leave one out cross-validation to prevent overfitting. After performing the random search over $n = 10$ iterations to optimize classification accuracy, the best hyperparameters were selected. These hyperparameters were then used and a leave-one-out cross validation procedure was used to assess the overall accuracy of the classifier (percentage of trials correctly classified). This randomized hyperparameter search and final accuracy assessment were performed separately for each update trial type. As a control, the randomized search and cross validation were also performed with randomly shuffled target (choice) labels n = 1000 times. The significance of the classifier was assessed by testing whether the classifier outperformed 95% of the distribution of accuracies from the shuffled classifier (permutation test).

Statistical analyses

We used a linear mixed-effects models (LME) approach to assess the significance of differences while controlling for repeated measures from the same animals and sessions. In our model, our variables of interest such as decoding output or single unit firing rates were included as our fixed effects. We set our random effects as session-nested-in-animal random effects with random intercepts at both levels. Statistical significance was first estimated with an ANOVA with Kenward-Roger's methods to determine whether the predictors had any significant effect. If the F-test was statistically significant, we then performed pairwise comparisons to assess significant differences using estimated marginal means and reported Tukey-adjusted p-values. For one-sample analyses, we used a Wilcoxon signed rank test. For correlation analyses, we calculated the Spearman rank-order correlation coefficient. All statistical tests were two-sided unless stated otherwise. Details on specific statistical parameters and the values of sample size n are described in the figure legends and statistical table (Supplementary Table 2). Note that the LME statistical approach considers the hierarchical nature of the data, rather than taking a mean per session or treating each sample independently. Existing visualization methods do not exactly show this hierarchical information. Therefore, we report multiple types of information about the underlying distributions including the means and 95% confidence intervals computed with $n = 1000$ bootstrap samples for sessions shown in the figures, the means and standard error of the means for trials reported in the figure legends, and the minimum, 25th percentile, median, 75th percentile, and maximum for trials reported in Supplementary Table 2. Sample sizes were not predetermined but are similar to sample sizes used in the field. We recorded from a large number of single units (at least 600 from each animal) from multiple animals and analyzed their activity and determined significance. *P*-values reported as $p < 4.462e\text{-}61$ reflect the limits of R's numerical precision and represent very small values.

Analyses were performed using custom pipelines in MATLAB 2021-2022, Python 3.9, and R 4.1 with the following libraries: NumPy 1.26, SciPy 1.13, Matplotlib 3.8, Scikit-learn 1.4, Pandas 1.4, Tensorflow 2.16, Pynapple 0.2, nwbwidgets 0.8, pynwb 2.6, seaborn 0.11, track-linearization 2.3, pingouin 0.5, statannotations 0.5, statsmodels 0.14, lme4 1.1, lmerTest 3.1, emmeans 1.8, SHARP-Track @git620c449, Kilosort2, Phy 2.0, CellExplorer 1.2.

Reporting summary

Further information on research design is available in the Nature Portfolio Reporting Summary linked to this article.

Data availability

The raw data, processed data, and associated metadata generated in this study have been deposited in the DANDI (Distributed Archives for Neurophysiology Data Integration) data archive [RRID:SCR_017571] under the accession code dandiset 001371: https://dandiarchive.org/dandiset/001371. The data were uploaded in the NWB format[52] and organized into a BIDS-like structure[53]. Source data are provided with this paper.

Code availability

Custom code is available on GitHub: https://github.com/stephprince/update-project.

References

1. Tolman, E. C. Cognitive maps in rats and men. *Psychol. Rev.* **55**, 189–208 (1948).
2. Behrens, T. E. J. et al. What Is a Cognitive Map? Organizing Knowledge for Flexible Behavior. *Neuron* **100**, 490–509 (2018).
3. O'Keefe, J. & Nadel, L. *The Hippocampus as a Cognitive Map* (Clarendon Press; Oxford University Press, 1978).
4. Hunt, L. T. et al. Formalizing planning and information search in naturalistic decision-making. *Nat. Neurosci.* **24**, 1051–1064 (2021).
5. Pezzulo, G., Donnarumma, F., Maisto, D. & Stoianov, I. Planning at decision time and in the background during spatial navigation. *Curr. Opin. Behav. Sci.* **29**, 69–76 (2019).
6. Buckner, R. L. The role of the hippocampus in prediction and imagination. *Annu. Rev. Psychol.* **61**, 27–48 (2010).
7. Comrie, A. E., Frank, L. M. & Kay, K. Imagination as a fundamental function of the hippocampus. *Philosoph. Trans. R. Soc. B Biol. Sci.* **377**, 20210336 (2022).
8. Mullally, S. L. & Maguire, E. A. Memory, imagination, and predicting the future. *Neuroscientist* **20**, 220–234 (2014).
9. Redish, A. D. Vicarious trial and error. *Nat. Rev. Neurosci.* **17**, 147–159 (2016).
10. Lisman, J. & Redish, A. D. Prediction, sequences and the hippocampus. *Philos. Trans. R. Soc. B: Biol. Sci.* **364**, 1193–1201 (2009).
11. Johnson, A. & Redish, A. D. Neural ensembles in CA3 transiently encode paths forward of the animal at a decision point. *J. Neurosci.* **27**, 12176–12189 (2007).
12. Wikenheiser, A. M. & Redish, A. D. Hippocampal theta sequences reflect current goals. *Nat. Neurosci.* **18**, 289–294 (2015).
13. Feng, T., Silva, D. & Foster, D. J. Dissociation between the experience-dependent development of hippocampal theta sequences and single-trial phase precession. *J. Neurosci.* **35**, 4890–4902 (2015).
14. Foster, D. J. & Wilson, M. A. Hippocampal theta sequences. *Hippocampus* **17**, 1093–1099 (2007).
15. Gupta, A. S., Van Der Meer, M. A. A., Touretzky, D. S. & Redish, A. D. Segmentation of spatial experience by hippocampal theta sequences. *Nat. Neurosci.* **15**, 1032–1039 (2012).
16. Skaggs, W. E., McNaughton, B. L., Wilson, M. A. & Barnes, C. A. Theta phase precession in hippocampal neuronal populations and the

compression of temporal sequences. *Hippocampus* **6**, 149–72 (1996).
17. Wang, Y., Romani, S., Lustig, B., Leonardo, A. & Pastalkova, E. Theta sequences are essential for internally generated hippocampal firing fields. *Nat. Neurosci.* **18**, 282–288 (2014).
18. Wikenheiser, A. M. & Redish, A. D. Hippocampal sequences link past, present, and future. *Trends Cogn. Sci.* **16**, 361–362 (2012).
19. Kapl, S., Tichanek, F., Zitricky, F. & Jezek, K. Context-independent expression of spatial code in hippocampus. *Sci. Rep.* **12**, 20711 (2022).
20. Yu, J. Y. & Frank, L. M. Prefrontal cortical activity predicts the occurrence of nonlocal hippocampal representations during spatial navigation. *PLoS Biol.* **19**, e3001393 (2021).
21. Kay, K. et al. Constant sub-second cycling between representations of possible futures in the hippocampus. *Cell* **180**, 552–567.e25 (2020).
22. Wikenheiser, A. M. & Redish, A. D. Decoding the cognitive map: Ensemble hippocampal sequences and decision making. *Curr. Opin. Neurobiol.* **32**, 8–15 (2014).
23. Zheng, C., Hwaun, E., Loza, C. A. & Colgin, L. L. Hippocampal place cell sequences differ during correct and error trials in a spatial memory task. *Nat. Commun.* **12**, 3373 (2021).
24. Tamura, M., Spellman, T. J., Rosen, A. M., Gogos, J. A. & Gordon, J. A. Hippocampal-prefrontal theta-gamma coupling during performance of a spatial working memory task. *Nat. Commun.* **8**, 2182 (2017).
25. Jones, M. W. & Wilson, M. A. Theta rhythms coordinate hippocampal-prefrontal interactions in a spatial memory task. *PLoS Biol.* **3**, e402 (2005).
26. Hyman, J. M., Zilli, E. A., Paley, A. M. & Hasselmo, M. E. Medial prefrontal cortex cells show dynamic modulation with the hippocampal theta rhythm dependent on behavior. *Hippocampus* **15**, 739–749 (2005).
27. Benchenane, K. et al. Coherent theta oscillations and reorganization of spike timing in the hippocampal-prefrontal network upon learning. *Neuron* **66**, 921–936 (2010).
28. O'Neill, P.-K., Gordon, J. A. & Sigurdsson, T. Theta oscillations in the medial prefrontal cortex are modulated by spatial working memory and synchronize with the hippocampus through its ventral subregion. *J. Neurosci.* **33**, 14211–14224 (2013).
29. den Bakker, H., Van Dijck, M., Sun, J.-J. & Kloosterman, F. Sharp-wave-ripple-associated activity in the medial prefrontal cortex supports spatial rule switching. *Cell Rep.* **42**, 112959 (2023).
30. Berners-Lee, A., Wu, X. & Foster, D. J. Prefrontal cortical neurons are selective for non-local hippocampal representations during replay and behavior. *J. Neurosci.* **41**, 5894–5908 (2021).
31. Hasz, B. M. & Redish, A. D. Spatial encoding in dorsomedial prefrontal cortex and hippocampus is related during deliberation. *Hippocampus* **30**, 1194–1208 (2020).
32. Tang, W., Shin, J. D. & Jadhav, S. P. Multiple time-scales of decision-making in the hippocampus and prefrontal cortex. *Elife* **10**, e66227 (2021).
33. Guise, K. G. & Shapiro, M. L. Medial prefrontal cortex reduces memory interference by modifying hippocampal encoding. *Neuron* **94**, 183–192.e8 (2017).
34. Schmidt, B., Duin, A. A. & Redish, A. D. Disrupting the medial prefrontal cortex alters hippocampal sequences during deliberative decision making. *J. Neurophysiol.* **121**, 1981–2000 (2019).
35. Jezek, K., Henriksen, E. J., Treves, A., Moser, E. I. & Moser, M. B. Theta-paced flickering between place-cell maps in the hippocampus. *Nature* **478**, 246–249 (2011).
36. O'Keefe, J. & Recce, M. L. Phase relationship between hippocampal place units and the EEG theta rhythm. *Hippocampus* **3**, 317–330 (1993).
37. Tseng, S.-Y., Chettih, S. N., Arlt, C., Barroso-Luque, R. & Harvey, C. D. Shared and specialized coding across posterior cortical areas for dynamic navigation decisions. *Neuron* **110**, 2484–2502.e16 (2022).
38. Gillespie, A. K. et al. Hippocampal replay reflects specific past experiences rather than a plan for subsequent choice. *Neuron* **109**, 3149–3163.e6 (2021).
39. Wang, M., Foster, D. J. & Pfeiffer, B. E. Alternating sequences of future and past behavior encoded within hippocampal theta oscillations. *Science (1979)* **370**, 247–250 (2020).
40. Zielinski, M. C., Shin, J. D. & Jadhav, S. P. Coherent coding of spatial position mediated by theta oscillations in the hippocampus and prefrontal cortex. *J. Neurosci.* **39**, 4550–4565 (2019).
41. Kaefer, K., Nardin, M., Blahna, K. & Csicsvari, J. Replay of Behavioral Sequences in the Medial Prefrontal Cortex during Rule Switching. *Neuron* **106**, 154–165 (2020).
42. Tang, W., Shin, J. D. & Jadhav, S. P. Geometric transformation of cognitive maps for generalization across hippocampal-prefrontal circuits. *Cell Rep.* **42**, 112246 (2023).
43. Sarel, A. et al. Natural switches in behaviour rapidly modulate hippocampal coding. *Nature* **609**, 119–127 (2022).
44. Aronov, D. & Tank, D. W. Engagement of neural circuits underlying 2D spatial navigation in a rodent virtual reality system. *Neuron* **84**, 442–456 (2014).
45. Pinto, L., et al. An accumulation-of-evidence task using visual pulses for mice navigating in virtual reality. *Front. Behav. Neurosci.* **12**, 36 (2018).
46. Hu, F., Zhang, L.-X. & He, X. Efficient randomized-adaptive designs. *Ann Stat.* **37**, 2543–2560 (2009).
47. Shamash, P., Carandini, M., Harris, K. & Steinmetz, N. A tool for analyzing electrode tracks from slice histology. Preprint at *biorxiv* https://doi.org/10.1101/447995 (2018).
48. Pachitariu, M., Steinmetz, N., Kadir, S., Carandini, M. & Harris, K. D. Kilosort: realtime spike-sorting for extracellular electrophysiology with hundreds of channels. Preprint at *bioRxiv* https://doi.org/10.1101/061481 (2016).
49. Petersen, P. C., Siegle, J. H., Steinmetz, N. A., Mahallati, S. & Buzsáki, G. CellExplorer: A framework for visualizing and characterizing single neurons. *Neuron* **109**, 3594–3608.e2 (2021).
50. Viejo, G. et al. Pynapple, a toolbox for data analysis in neuroscience. *ELife* **12**, RP85786 (2023).
51. Saleem, A. B., Diamanti, E. M., Fournier, J., Harris, K. D. & Carandini, M. Coherent encoding of subjective spatial position in visual cortex and hippocampus. *Nature* https://doi.org/10.1038/s41586-018-0516-1 (2018).
52. Rübel, O. et al. The Neurodata Without Borders ecosystem for neurophysiological data science. *Elife* **11**, e78362 (2022).
53. Gorgolewski, K. J. et al. The brain imaging data structure, a format for organizing and describing outputs of neuroimaging experiments. *Sci Data* **3**, 160044 (2016).

Acknowledgements

We thank Shantanu Jadhav for helpful feedback and all members of the Singer laboratory for technical assistance and feedback on the paper. We thank Bailey Mariner and scidraw.io for illustrations. This work was supported by NSF GRFP grant DGE-1444932, NIH grant T32NS096050-22, and the Emory University Women's Club Graduate Research Fellowship (to S.M.P.); the Georgia Institute of Technology President's Undergraduate Research Fellowship (to N.K. and T.A.Y.); the National Institutes of Health (NIH)-National Institute of Neurological Disorders and Stroke Grants R01 NS109226 and 2RF1NS109226, the NIH National Institute of Aging Grant RF1AG078736-01, Packard Award in Science and Engineering, McCamish Foundation, Friends and Alumni of Georgia Tech (to A.C.S.).

Author contributions

S.M.P. and A.C.S. conceptualized the study and developed methodology. S.M.P., T.A.Y., N.K., and T.C.R. carried out behavioral training. S.M.P. conducted electrophysiological recordings. S.M.P. and T.A.Y. curated data. S.M.P. and S.D.C. wrote code and analyzed the data. S.M.P., S.D.C., and A.C.S. wrote the paper. A.C.S. supervised the project and acquired funding.

Competing interests

The authors declare no competing interests.

Additional information

Supplementary information The online version contains supplementary material available at https://doi.org/10.1038/s41467-025-60122-8.

Correspondence and requests for materials should be addressed to Annabelle C. Singer.

Peer review information *Nature Communications* thanks Eun Jung Hwang and the other, anonymous, reviewer for their contribution to the peer review of this work.